**Atmospheric
Chemistry
and Physics**

# The chemistry of OH and HO$_2$ radicals in the boundary layer over the tropical Atlantic Ocean

**L. K. Whalley**[1,5]**, K. L. Furneaux**[1,†]**, A. Goddard**[1]**, J. D. Lee**[2,6]**, A. Mahajan**[1]**, H. Oetjen**[1]**, K. A. Read**[2,6]**, N. Kaaden**[3]**, L. J. Carpenter**[2]**, A. C. Lewis**[2,6]**, J. M. C. Plane**[1]**, E. S. Saltzman**[4]**, A. Wiedensohler**[3]**, and D. E. Heard**[1,5]

[1]School of Chemistry, University of Leeds, Woodhouse Lane, Leeds, LS2 9JT, UK
[2]Chemistry Department, University of York, Heslington, YO10 5DD, UK
[3]Physics Department, Leibniz Institute for Tropospheric Research, Leipzig, Germany
[4]Department of Earth System Science, University of California, Irvine, CA, USA
[5]National Centre for Atmospheric Sciences, University of Leeds, Leeds, LS2 9JT, UK
[6]National Centre for Atmospheric Sciences, University of York, Heslington, YO10 5DD, UK
[†]Sadly passed away 28 July 2009

**Abstract.** Fluorescence Assay by Gas Expansion (FAGE) has been used to detect ambient levels of OH and HO$_2$ radicals at the Cape Verde Atmospheric Observatory, located in the tropical Atlantic marine boundary layer, during May and June 2007. Midday radical concentrations were high, with maximum concentrations of $9 \times 10^6$ molecule cm$^{-3}$ and $6 \times 10^8$ molecule cm$^{-3}$ observed for OH and HO$_2$, respectively. A box model incorporating the detailed Master Chemical Mechanism, extended to include halogen chemistry, heterogeneous loss processes and constrained by all available measurements including halogen and nitrogen oxides, has been used to assess the chemical and physical parameters controlling the radical chemistry. The model was able to reproduce the daytime radical concentrations to within the 1 $\sigma$ measurement uncertainty of 20% during the latter half of the measurement period but significantly under-predicted [HO$_2$] by 39% during the first half of the project. Sensitivity analyses demonstrate that elevated [HCHO] ($\sim$2 ppbv) on specific days during the early part of the project, which were much greater than the mean [HCHO] (328 pptv) used to constrain the model, could account for a large portion of the discrepancy between modelled and measured [HO$_2$] at this time. IO and BrO, although present only at a few pptv, constituted $\sim$19% of the instantaneous sinks for HO$_2$, whilst aerosol uptake and surface deposition to the ocean accounted for a further 23% of the HO$_2$ loss at noon. Photolysis of HOI and HOBr accounted for $\sim$13% of the instantaneous OH formation. Taking into account that halogen oxides increase the oxidation of NO$_x$ (NO $\rightarrow$ NO$_2$), and in turn reduce the rate of formation of OH from the reaction of HO$_2$ with NO, OH concentrations were estimated to be 9% higher overall due to the presence of halogens. The increase in modelled OH from halogen chemistry gives an estimated 9% shorter lifetime for methane in this region, and the inclusion of halogen chemistry is necessary to model the observed daily cycle of O$_3$ destruction that is observed at the surface. Due to surface losses, we hypothesise that HO$_2$ concentrations increase with height and therefore contribute a larger fraction of the O$_3$ destruction than at the surface.

## 1 Introduction

The OH radical is one of the most dominant oxidants in the troposphere. It is most prevalent in tropical regions where high levels of humidity and solar irradiance lead to high rates of OH production:

$$O_3 + h\nu(\lambda < 340 \text{ nm}) \rightarrow O_2 + O(^1D) \quad \text{(R1)}$$

$$O(^1D) + H_2O \rightarrow 2 \, OH \quad \text{(R2)}$$
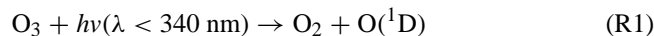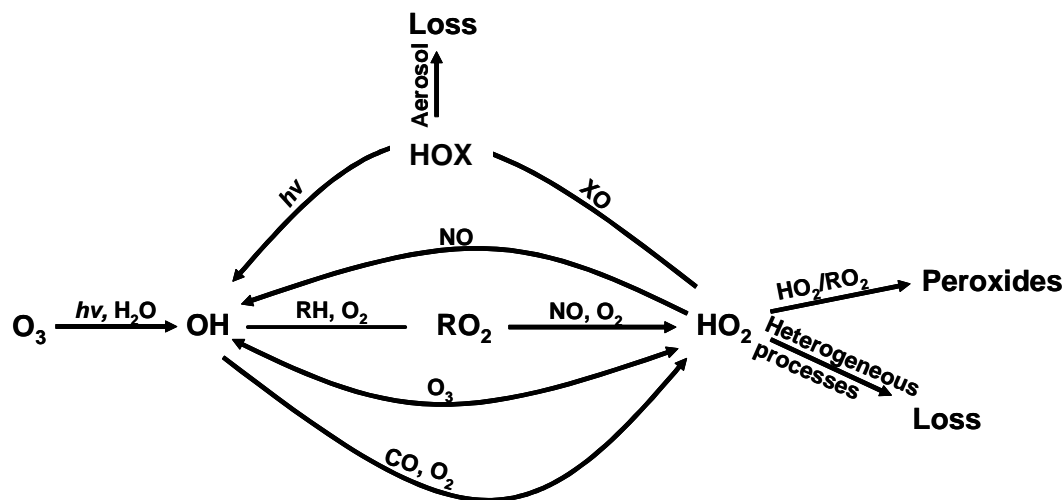
**Fig. 1.** Chemical reaction scheme showing the reactions affecting OH and HO$_2$ concentrations in the remote MBL. X=I, Br and R= alkyl group.

Around 80% of methane, the third most abundant greenhouse gas, is processed within the tropical troposphere by the OH radical with the tropical marine lower troposphere contributing ∼25% to the total tropospheric methane removal rate (Bloss et al., 2005a). The loss of methane is disproportionately high in the lower tropical troposphere compared to at higher altitudes in the tropical troposphere owing to the large temperature dependence of the reaction between methane and OH; the reaction rate is ∼24 times greater at the surface than at the tropopause in the tropics.

Despite the importance of the lower marine tropical troposphere, OH measurements in this region, and also those of HO$_2$, which is closely coupled to OH through the reaction cycles shown in Fig. 1, are sparse. Aircraft measurements of OH and HO$_2$ were made during the Pacific Exploratory Missions (PEM) (Hoell et al., 1996, 1997, 1999; Raper et al., 2001), with OH midday concentrations between 6–8×10$^6$ molecule cm$^{-3}$ recorded in the tropical marine boundary layer (MBL) using the Selected Ion Chemical Ionisation Mass Spectrometer (SICIMS) technique (Mauldin III et al., 1999, 2001). Modelling studies (using a photochemical box model and a photostationary state point model) indicated that Reaction (R2) was the major source of HO$_x$ (OH+HO$_2$) (contributing 81%), while the major sinks involved the formation and subsequent loss of the peroxides of H$_2$O$_2$ and CH$_3$OOH (Chen et al., 2001). The models under-predicted the measured MBL OH by 15–20%; no halogen chemistry was included in these models. The primary focus of many of the PEM campaigns was the free-troposphere, and so measurements in the boundary layer were limited. OH measurements using Differential Optical Absorption Spectroscopy (DOAS) have been made onboard the R/V Polarstern, as part of the Air Chemistry and Lidar Studies of Tropospheric and Stratospheric Species on the Atlantic Ocean (ALBATROSS) project held in October/November 1996 (Brauers et al., 2001). OH data were collected over the latitudinal range 5° N to 40° S in the Atlantic. OH displayed a distinct diurnal profile with a maximum around local noon of ∼7×10$^6$ molecule cm$^{-3}$. A simple photochemical box model, containing just CO and methane as sinks for OH, on average underpredicted OH by 16%, but was within the combined calibration errors associated with the OH, CO and photolysis frequency measurements.

In background marine airmasses, which are low in volatile organic compounds (VOCs) and NO$_x$, with HO$_x$ generated mainly by Reactions (R1)–(R2) and removed primarily by the formation and subsequent loss of peroxides, modelled and measured OH concentrations are in reasonable agreement. In contrast to OH, however, models often significantly overpredict HO$_2$ in such airmasses when only this basic chemistry is considered (Sommariva et al., 2004, 2006; Kanaya et al., 2007).

The Southern Ocean Photochemistry Experiment (SOAPEX-2) was held at Cape Grim, in North Western Tasmania, Australia, in 1999 under extremely clean conditions ([NO]<3 pptv). Two chemical schemes were constructed to describe the free-radical budget; one containing just the oxidation of CO and methane, the other also describing the oxidation of non-methane hydrocarbons (NMHC) that were also measured (Sommariva et al., 2004). Box model calculations of [OH] using these two mechanisms agreed to within 5–10%, implying a minor role for NMHC as an OH sink, and both over-predicted [OH] by 10–20%. [HO$_2$], however, was overestimated by up to 40%, but model agreement was improved by assuming an HO$_2$ uptake coefficient to aerosol of unity (Sommariva et al., 2004). This, however, is probably an unreasonable assumption, as recent experimentally determined uptake coefficients for

HO$_2$ on realistic aerosol surfaces range only from 0.01–0.1 (Thornton et al., 2008; Taketani et al., 2008, 2009). During the summer 2002 NAMBLEX project, which took place at Mace Head on the West coast of Ireland, the role of halogen oxides, specifically IO and BrO, in the chemistry of the MBL was confirmed (Bloss et al., 2005b; Sommariva et al., 2006; Smith et al., 2006). IO and BrO react quickly with HO$_2$, with rate coefficients at 25° C of 8.6 and $2.1 \times 10^{-11}$ molecule$^{-1}$ cm$^3$ s$^{-1}$ for IO and BrO, respectively (IUPAC, 2006). The HOI and HOBr formed may then either undergo photolysis to yield OH (and a halogen atom) or be taken up onto an aerosol surface. Reaction of HOI and HOBr with halide ions in acidified aerosol can form volatile inter-halogen species (Vogt et al., 1996; Pechtl et al., 2007) which photolyse in the gas phase allowing gaseous halogen chemistry to continue. The inclusion of a halogen scheme has been shown to improve the HO$_2$ modelled to measured agreement at a number of marine sites (Bloss et al., 2005b; Smith et al., 2006; Sommariva et al., 2006; Kanaya et al., 2007), and could account for the model discrepancy reported during the SOAPEX-2 experiment if realistic HO$_2$ uptake coefficients were instead used (Haggerstone et al., 2005).

At coastal locations such as Mace Head, the primary source of IO is the photolysis of molecular iodine (Saiz-Lopez and Plane, 2004) and, to a smaller extent, iodocarbons (Chameides and Davis, 1980; Carpenter et al., 1999), which are released by macro-algae exposed at low tide. The iodine atoms generated react rapidly with O$_3$ to generate the IO radical. At coastal sites where macro-algae are exposed, IO follows a distinct diurnal profile, with concentrations peaking with low tide during the daytime (Alicke et al., 1999; Whalley et al., 2007). The impact of halogens on tropospheric oxidants in regions without tidally exposed macro-algae, for example the open ocean, which covers ∼70% of Earth's surface, was until recently, unconfirmed. A number of theoretical and observational studies had inferred indirectly the possible global impact of halogens (Dickerson et al., 1999; Vogt et al., 1999; Galbally et al., 2000; von Glasow et al., 2002; von Glasow et al., 2004), but observations in the remote MBL were limited (Allan et al., 2000; Leser et al., 2003). In 2006/2007 an 8 month measurement series of IO and BrO at the Cape Verde Atmospheric Observatory (CVAO) was reported (Read et al., 2008), exhibiting broad diurnal profiles following light intensity; with typical peak concentrations of ∼1.4 and 2.5 pptv, respectively. CVAO is thought to be representative of the open ocean tropical MBL; ship and aircraft measurements confirm that the measurements at the site are representative of the surrounding area (Read et al., 2008; Lee et al., 2009a) and hence these observations suggest a potentially global presence of halogen oxides. Although IO and BrO are present at much lower concentrations than observed at coastal sites, for example Mace Head ([BrO]$_{max}$=6.5 pptv; Saiz-Lopez et al., 2004, and [IO]$_{max}$∼30 pptv; Commane, 2009) and Roscoff, France ( [IO]$_{max}$∼28 pptv; Furneaux et al., 2009), the inclusion of bromine and iodine chemistry was

necessary to model adequately the daily O$_3$ destruction that is observed at Cape Verde (Read et al., 2008).

For [NO]<∼20 pptv, O$_3$, an important greenhouse gas in the troposphere, is photochemically destroyed (Penkett et al., 1997; Lee et al., 2009b) (e.g. via Reactions (R1)–(R4) and as shown in Fig. 1).

$$O_3 + OH \rightarrow HO_2 + O_2 \qquad \text{(R3)}$$

$$O_3 + HO_2 \rightarrow OH + 2O_2 \qquad \text{(R4)}$$
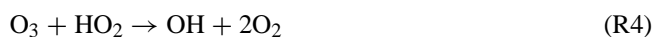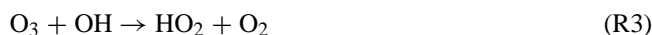
When halogen oxides are present, further O$_3$ destruction may occur via the reaction of a halogen atom (X) with O$_3$ and subsequent reaction of XO with HO$_2$, NO, or XO:

$$X + O_3 \rightarrow XO + O_2 \qquad \text{(R5)}$$

$$XO + HO_2 \rightarrow HOX + O_2 \qquad \text{(R6a)}$$

$$HOX + h\nu \rightarrow OH + X \qquad \text{(R6b)}$$

$$XO + NO \rightarrow X + NO_2 \qquad \text{(R7)}$$

$$XO + IO \rightarrow X + OIO \qquad \text{(R8)}$$

$$XO + XO \rightarrow 2X + O_2 \qquad \text{(R9)}$$

Surface deposition of O$_3$ may also contribute to its destruction in the BL. At higher levels of NO the regime switches to a net O$_3$ production via the following reactions:

$$HO_2 + NO \rightarrow OH + NO_2 \qquad \text{(R10)}$$

$$RO_2 + NO \rightarrow RO + NO_2 \qquad \text{(R11)}$$

$$NO_2 + h\nu(\lambda < 420\,nm) \rightarrow NO + O \qquad \text{(R12)}$$

$$O + O_2 + M \rightarrow O_3 + M \qquad \text{(R13)}$$

Read et al. (2008) reported a consistent daytime O$_3$ destruction cycle at the CVAO with an annually averaged loss of $3.3 \pm 2.6$ ppbv d$^{-1}$. In this paper, we present OH and HO$_2$ measurements made at the observatory as part of the Reactive Halogen in the Marine Boundary Layer (RHaMBLe) project (Lee et al., 2009a). The contribution towards the overall O$_3$ destruction from the reactions of OH and HO$_2$ radicals with O$_3$ is determined directly. A detailed model is used to investigate the impact of the reactions of HO$_2$ with BrO and IO, and the subsequent recycling to OH via the photolysis of HOBr and HOI. Of interest is the contribution of halogen chemistry to the rate of photochemical destruction of O$_3$ and the budgets of OH and HO$_2$ radicals. The significance of halogen chemistry for the global oxidising capacity and hence the removal rate of methane is also examined.
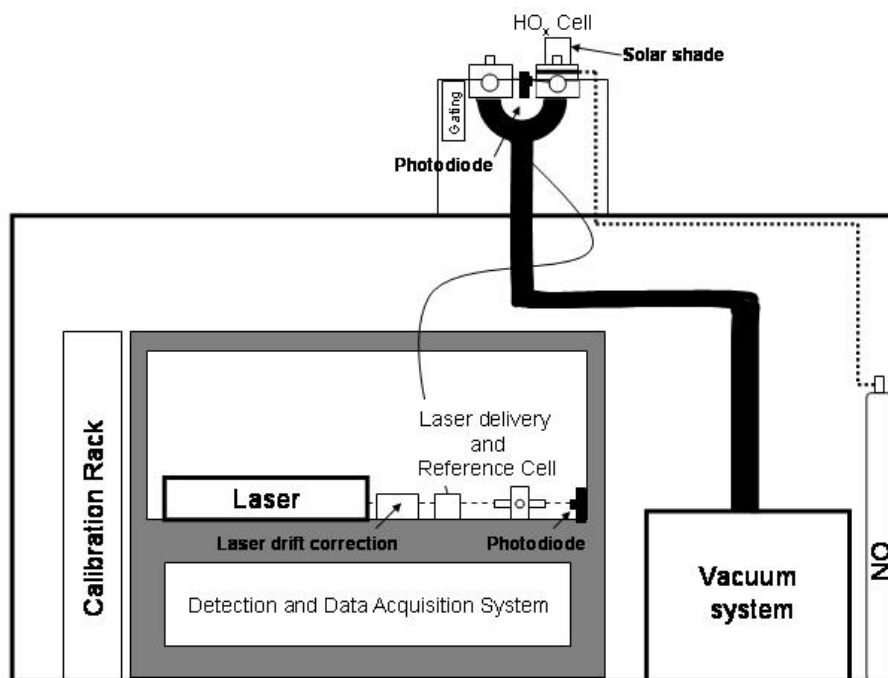
**Fig. 2.** Schematic of the FAGE laboratory set-up during RHaMBLe (see text for details).

## 2 Experimental

### 2.1 Measurement of OH and HO₂ radicals

Fluorescence Assay by Gas Expansion (FAGE) provides a powerful method for the detection of tropospheric OH and HO₂ radicals (Heard and Pilling, 2003). The technique utilises the strong $A^2\Sigma^+$ (v′=0)←$X^2\Pi_i$(v″=0) $Q_1$(2) transition at 308 nm for OH laser excitation. HO₂ can also be detected by this method following initial chemical conversion to OH by adding NO and subsequent detection. Laser-induced fluorescence experiments of this type are conducted at low pressures (∼133 Pa) to extend the fluorescence lifetime of the OH radical sufficiently to allow the fluorescence to be discriminated from the more intense laser radiation. This is achieved by temporal gating of the detector; a channel photo multiplier (CPM) (Perkin Elmer C943P) is used. Switching the CPM off during the laser pulse also helps to prevent detector saturation (Smith et al., 2006). OH fluorescence and scattered light (laser and solar) are recorded by a gated photon counter (SRS SR400) during a 500 ns integration period (Gate A), commencing approximately 50 ns after the end of the laser pulse (FWHM∼35 ns). A small fraction of the total laser scattered light, along with solar scattered light and detector dark counts constitute a background signal to the OH fluorescence in gate A. The contribution of the solar scattered light and dark counts can be determined using a second photon counting gate (Gate B), delayed by 50 μs from the first, at a time when the fluorescence and laser pulse have

subsided. Tuning the laser away from resonance with the OH transition (online), to a wavelength where OH does not absorb (offline), allows the signal contribution of the laser scatter to be determined.

Ambient OH and HO₂ measurements have been made using the University of Leeds ground-based FAGE instrument since 1996 (Heard and Pilling, 2003). Details of the instrument have previously been reported (Smith et al., 2006), and are only considered briefly here. The operating conditions encountered at the CVAO were challenging and a modified operating procedure was necessary. The instrument is housed in an instrumented 20 ft sea container (Fig. 2), and comprises a laser system, an OH reference cell for calibration of the laser wavelength, fluorescence cells which are housed on the roof of the sea container at a height of 3.5 m, and data acquisition and calibration systems.

During the RHaMBLe project, the instrument was located at the CVAO (16.85° N, 24.87° W), at Calhau on a northeast facing rocky foreshore on the island of São Vicente within the Cape Verde archipelago. The island shores shelve steeply and very little tidal variability is apparent near to the site. A detailed map of Cape Verde and the layout of the site can be found in Lee et al. (2009a). The site is adjacent to the ocean, the University of Leeds ground-based FAGE instrument was approximately 50 m from the water's edge and the inlet was positioned approximately 3.5 m above sea level (a.s.l.). A wavelength tuneable Nd:YAG pumped Ti:Sapphire laser (Photonics Industries DS 20-532) was used to generate UV light at 308 nm. The Nd:YAG produces ∼9 W of

532 nm radiation at a pulse repetition rate of 5 kHz, and is used to pump a Ti:Sapphire laser which generates up to 1.6 W of broadband near-IR radiation. Selecting a wavelength close to 924 nm, by changing the incident angle of an intra-cavity diffraction grating, and frequency tripling, by passing the light through two non-linear harmonic generation stages, generates the required radiation close to 308 nm for OH excitation. The time taken for the Ti:Sapphire laser to build up sufficient gain for laser output was found to change significantly in this campaign. When optimally aligned, the delay between the 532 nm pump pulse and the Ti:Sapphire laser output can be as short as 200 ns, but as laser optics become damaged or alignment shifts (possibly due to temperature changes) this delay can increase. The time between the Ti:Sapphire laser pulse, $t_{308}$, and the time when the fluorescence photons are counted (beginning of gate A) is critical, and must be maintained constant to ensure that the instrument sensitivity and background laser scatter does not change. A counter timer (Agilent Technologies, 225 MHz universal counter) triggered at the same time ($t_0$), as the laser, and coupled to a photodiode (Hamamatsu, S6468 series), which monitors the onset of the pulse of frequency tripled 308 nm light ($t_{308}$), was implemented during this project to measure the delay $t_{308} - t_0$. This system allowed any drift in $t_{308} - t_0$ to be directly monitored in real time and a correction added to or subtracted from the time of the trigger controlling the start of the fluorescence photon counting gate A. The correction was applied prior to the beginning of each data acquisition cycle, which lasted ∼450 s.

During this campaign a number of the optical coatings within the laser became damaged as a result of the high intensity laser beam hitting dust or sea-salt particles that had deposited on the optics. Although this problem occurs, to a certain extent, in all environments, the effect was particularly exacerbated at the CVAO, which is exposed to the elements being close to the water's edge and subject to wind-speeds regularly in excess of 10 ms$^{-1}$. The resultant optical damage led to a reduction in laser power at 308 nm from ∼40 mW to <20 mW as the project progressed. The stability of the delay time $t_{308} - t_0$ was significantly worse than had been observed previously (or since). In addition, tuning the laser wavelength by 0.006 nm (the interval between the online and offline positions) significantly changed $t_{308} - t_0$ and hence the position of gate A relative to the laser. As a result, the laser power and hence the laser scattered light changed significantly between the online and offline positions. The timing drift precluded OH measurements during the first half of the project, and the HO$_2$ measurements were subject to a larger uncertainty during this period. The timing problem was eventually ameliorated by reducing the interval between the online and offline wavelengths to 0.004 nm, for which the change in $t_{308} - t_0$ was much reduced.

Upon exiting the laser, the light was split by a dielectrically coated beam-splitter (CVI Optics Ltd). 80% was directed to a fluorescence cell via a fibre launcher (Elliot Gold$^{TM}$ series), fibre optic (Elliot Scientific) and collimation assembly (Oz Optics), and 19% to an OH reference cell, designed to aid the precise tuning of the laser wavelength to the peak of the Q$_1$(2) OH transition. A large concentration of OH is generated by the pyrolysis of H$_2$O vapour, using a flow of humidified air over a heated filament. Light exiting the reference cell was directed on a UV sensitive photodiode (New Focus 2032) to determine the laser power for subsequent normalisation of the ambient LIF signal; a cut-off filter was placed in front of the photodiode to prevent visible light reaching it. The remaining UV light (1%) was directed onto a fast photodiode (Hamamatsu, S6468 series), which was used as input to the counter-timer to correct for any drift in the laser timing.

The laser light entered the detection cell on the roof of the container via a baffled side arm and intersected the ambient air stream, drawn through a 0.8 mm diameter nozzle sat on a 25 mm turret, on an axis perpendicular to the fluorescence detection axis containing the CPM. The laser light then exited the cell via a second baffled side arm and was reflected onto a second UV sensitive filtered photodiode (New Focus 2032), the output of which was monitored to check good laser alignment was being maintained through the cell. Ambient temperature fluctuations can cause the voltage output from photodiodes to drift, this precludes the use of the detection cell photodiode (located on the roof) to normalise the LIF signal to laser power. High solar intensities were experienced at the Cape Verde site (the solar zenith angle at solar noon in June at the site was ∼5°) leading to a large amount of solar scattered light detected within the cell by the CPM. A solar shade, consisting of a sheet of black aluminium (10 cm×10 cm) was placed 15 cm above the nozzle, which reduced the solar counts that reached the detector by an order of magnitude. Without the shade, solar counts at solar noon could reach >200 counts s$^{-1}$, the random fluctuations of which are larger than the typical signal from OH, making measurements extremely difficult. The windspeed at the site was ∼10 ms$^{-1}$ (and rarely dropped below 5 ms$^{-1}$), thus the average time an air parcel spent under the shade was ∼0.01 s, much shorter than the lifetime of either OH or HO$_2$ radicals, and should not perturb their concentrations.

Normally, the University of Leeds ground-based FAGE instrument utilises two fluorescence cells for simultaneous OH and HO$_2$ measurements (Smith et al., 2006). Due to low laser power, coupled with a CPM failure in the OH cell, however, only one cell was operable during the project and was used instead to make alternating sequential measurements of the two radicals. This set-up has been successfully utilised on a number of previous field projects, for example during the recent CHABLIS project (Bloss et al., 2007). Signals from the photon counter were integrated for 1 s periods. Online data were acquired for 200 s and consisted of 100 s of fluorescence from OH, followed by 100 s of fluorescence from both OH and converted HO$_2$ (NO added to the cell). The offline signal was then collected for a further period of 100 s, with

NO added after 50 s to measure any additional signal caused by the addition of NO, for example from enhanced scattering (there was no extra signal). The [OH] did not vary significantly during a single data acquisition period, and, therefore, the signal due to HO$_2$ could be determined by subtracting the OH online signal from the HO$_x$ online signal. In total, one data acquisition cycle (including the time taken to find the peak of the OH transition) took $\sim$450 s.

Calibrations were performed every two to three days throughout the campaign. A zero air generator (EcoPhysics PAG 003) was coupled to a zero air trap (Megatech CE-500KF-O-4R Gas Purifier) which reduced the levels of NO$_x$, VOCs and CO to <1 pptv and following humidification in a liquid water bubbler, this flow was directed down a 60 cm long quartz glass tube (internal diameter 22 cm) past a Hg pen-ray lamp (LOT Oriel model 6035), under roughly laminar flow conditions (Reynolds Number = 646). The 184.9 nm radiation emitted by the pen-ray lamp photolysed H$_2$O vapour, generating OH and HO$_2$ (in the presence of O$_2$) in equal quantities. A few ppbv of O$_3$ was generated from O$_2$ photolysis and the subsequent O+O$_2$ recombination reaction, and this was used as a chemical actinometer for the 184.9 nm flux. When calibrating for HO$_2$ a 100 sccm flow of CO (BOC, 1% CO in N$_2$) was added to the humidified air flow to rapidly convert all OH radicals to HO$_2$ ($\sim$2.5$\times$10$^{-3}$ s OH lifetime). Approximately 5 slm of the central portion of the flow within the tube was drawn into the detection cell, via the 0.8 mm sampling nozzle, the excess flow ($\sim$7 slm) was directed towards an O$_3$ analyser (Thermo Environmental Instruments – TEI – 42C) and Dewpoint Hygrometer (General Eastern 1311DR sensor). Determining [H$_2$O] and [O$_3$] enabled the radical concentration to be calculated using:

$$[OH] = [HO_2] = \frac{[O_3][H_2O]\sigma_{H_2O}\phi_{HO_x}}{[O_2]\sigma_{O_2}\phi_{O_3}P} \quad (1)$$

where $\sigma_{H_2O}$ and $\sigma_{O_2}$ are the 184.9 nm absorption cross sections of H$_2$O vapour and O$_2$, determined experimentally to be $(7.1\pm0.2)\times10^{-20}$ molecule$^{-1}$ cm$^2$ and $(1.37\pm0.14)\times10^{-20}$ molecule$^{-1}$ cm$^2$, respectively, for the same pen-ray lamp used during the field measurements. $\phi_{HO_x}$=1 is the quantum yield for production of OH or HO$_2$ in the absence of added CO, and $\phi_{HO_x}$=2 for HO$_2$ in the presence of added CO. $P$ is the profile factor, which is discussed further below. With the pen-ray lamp switched off ([HO$_x$]=0) it was found that there was no additional signal above the background when NO was added to the FAGE cell, ruling out the presence of any significant artefact due to HO$_x$ production either directly from photolysis of impurities (e.g. HNO$_3$) in the NO, or from the photolysis of species desorbed from the walls after exposure to NO.

A correction needs to be applied to account for the parabolic distribution of radial flow velocities across the calibration tube under laminar flow conditions. The central portion of the flow sampled by the detection cell has a higher velocity and hence spends less time in the photolysis region compared with the remainder of the flow (excess) that is sampled by the O$_3$ analyser from regions of the tube with a lower velocity. This radial flow distribution leads to more O$_3$ in the excess air relative to that in the FAGE sampled air at the centre. Any variability in the flux of the 184.9 nm light across the tube can also perturb the O$_3$ and radical profile in the tube. The profile factor, defined as $P$=[O$_3$]$_{excess}$/[O$_3$]$_{central}$, has been experimentally measured as 1.57$\pm$0.09 (Smith, 2007), and is used in Eq. (1) to calculate [OH] and [HO$_2$].

The sensitivity of the cell towards OH and HO$_2$, in units of cts s$^{-1}$ mW$^{-1}$ molecule$^{-1}$ cm$^3$, is given by:

$$C_{OH} = \frac{S_{OH}}{[OH]\times Pwr} \text{ and } C_{HO_2} = \frac{S_{HO_2}}{[HO_2]\times Pwr} \quad (2)$$

$S_{OH}$ and $S_{HO_2}$ are the measured fluorescence signals (cts s$^{-1}$) due to OH (in the absence of added CO and NO) and HO$_2$ (in the presence of added CO and NO), respectively. $Pwr$ is the laser power entering the cell in mW, which decreased from $\sim$19 to $\sim$7 mW during the RHaMBLe campaign. The average instrument sensitivity was $1.1\times10^{-7}$ cts s$^{-1}$ mW$^{-1}$ [OH]$^{-1}$ for OH and $4.4\times10^{-8}$ cts s$^{-1}$ mW$^{-1}$ [HO$_2$]$^{-1}$ for HO$_2$, with the 2 $\sigma$ uncertainty estimated as $\sim$40% for OH and HO$_2$ (Smith, 2007). The cell pressure was optimised for OH detection rather than for conversion of HO$_2$. The detection limit (LOD) is given by:

$$LOD = \frac{SNR}{Pwr\times C}\sqrt{\left(\frac{1}{m}+\frac{1}{n}\right)\frac{S_{back}}{t}} \quad (3)$$

where SNR is the signal-to-noise ratio (1), $m$ is the number of online data points (100), $n$ is the number of offline points (50), $S_{back}$ is the background signal comprising laser scattered light ($\sim$20 cts s$^{-1}$), solar scattered light (max. $\sim$20 cts s$^{-1}$ at noon) and CPM dark counts (0 cts s$^{-1}$) and $t$ is the integration of each data point (1 s). Using the above values and $Pwr$ = 9 mW, LODs of $1.1\times10^6$ molecule cm$^{-3}$ and $2.8\times10^6$ molecule cm$^{-3}$ were calculated for OH and HO$_2$, respectively.

## 2.2 Ancillary measurements

A number of ancillary measurements were made to permit a detailed characterisation of the atmospheric composition at the site and to constrain the box model. Details of these measurements are listed in Table 1 and are discussed further in Lee et al. (2009a). The majority of these measurements are part of a long term dataset made continuously at the Cape Verde Observatory since October 2006. The halogen oxide measurements made using Long Path-Differential Optical Absorption Spectroscopy (LP-DOAS) were part of an 8 month dataset, covering the period November 2006 to June 2007 (Read et al., 2008).

**Table 1.** Listing of the concurrent measurements made during the RHaMBLe project and used to constrain the box model.

| Measurements | Instrument | Typical noon value | Averaging Time | LOD (2 $\sigma$) | Reference |
|---|---|---|---|---|---|
| O$_3$ | TEI 42c, UV absorption | 35 ppbv | 1 min | 1 ppbv | (Lee et al., 2009a) |
| CO | Aerolaser, VUV resonance fluorescence | 104 ppbv | 1 min | – | (Lee et al., 2009a) |
| CH$_4$ | Flask Samples, Gas Chromatography analysis | 1821 ppbv | – | – | (Lee et al., 2009a) |
| NO | Chemiluminesence detector | 2.3 pptv | 1 h | 1.5 pptv | (Lee et al., 2009b) |
| NO$_2$ | Chemiluminesence detector | 11 pptv | 1 h | 4.1 pptv | (Lee et al., 2009b) |
| Ethane | Gas Chromatography- Flame Ionisation Detection (GC-FID) | 845±26 pptv | 1 h | 2.5 pptv | (Read et al., 2009) |
| Propane | GC-FID | 50±1.7 pptv | 1 h | 2.5 pptv | (Read et al., 2009) |
| Iso-butane | GC-FID | 2.2±0.2 pptv | 1 h | 2.5 pptv | (Read et al., 2009) |
| n-butane | GC-FID | 3.9±0.3 pptv | 1 h | 2.5 pptv | (Read et al., 2009) |
| Acetylene | GC-FID | 119±3.3 pptv | 1 h | 2.5 pptv | (Read et al., 2009) |
| Ethene | GC-FID | 21±1.4 pptv | 1 h | 2.5 pptv | (Read et al., 2009) |
| Propene | GC-FID | 22±0.9 pptv | 1 h | 2.5 pptv | (Read et al., 2009) |
| Isoprene | GC-FID | 10±1.0 pptv | 1 h | 1.0 pptv | (Read et al., 2009) |
| Acetaldehyde | GC-FID | 826±137 pptv | 1 h | 18 pptv | (Read et al., 2009) |
| Methanol | GC-FID | 749±115 pptv | 1 h | 7 pptv | (Read et al., 2009) |
| Acetone | GC-FID | 487±45 pptv | 1 h | 3 pptv | (Read et al., 2009) |
| IO | LP-DOAS | 1.3 pptv | 20–30 min | 0.3–0.5 pptv | (Read et al., 2008) |
| BrO | LP-DOAS | 2.9 pptv | 20–30 min | 0.5–1 pptv | (Read et al., 2008) |
| HCHO | LP-DOAS | 328 pptv | 20–30 min | 200 pptv | (Mahajan et al., 2010) |
| J(O$^1$D) | Filter Radiometer | $3.4 \times 10^{-5}$ s$^{-1 a}$ | 1 min | – | (Lee et al., 2009a) |
| Aerosol | Scanning Mobility Particle Sizer (SMPS) & Aerosol Particle Sizer (APS) | $1 \times 10^{-6}$ cm$^2$ cm$^{-3}$ | 30 min | – | (Allan et al., 2009) |
| Relative Humidity | Campbell Met Station | 76% | 1 min | – | (Lee et al., 2009a) |
| Temperature | Campbell Met Station | 296 K | 1 min | – | (Lee et al., 2009a) |
| Pressure | Campbell Met Station | 1016 hPa | 1 min | – | (Lee et al., 2009a) |

## 2.3 Box model using the master chemical mechanism

A box model was used to calculate OH and HO$_2$ concentrations, and contained a near explicit chemical scheme for the oxidative degradation of C1–C5 hydrocarbons, extracted from the Master Chemical Mechanism (MCM) version 3.1 (Saunders et al., 2003). The entire MCM treats the degradation of 135 VOCs and considers oxidation by OH, O$_3$ and NO$_3$. The degradation continues until CO$_2$ and H$_2$O vapour form as the final oxidation products. Complete details of the kinetic and photochemical data used in the mechanism are available at the MCM website (MCM, http://mcm.leeds.ac.uk/MCM/home). A halogen chemical scheme (listed in supplementary information: http://www.atmos-chem-phys.net/10/1555/2010/acp-10-1555-2010-supplement.pdf) was added to the MCM to assess the effect of IO, BrO and related species on the budgets of OH, HO$_2$ and O$_3$ concentrations. The mechanism contains photolysis of O$_3$, NO$_2$, HOI, HOBr, IO, aldehydes, ketones, H$_2$O$_2$ and organic hydroperoxides (RO$_2$H), but only measurements of $j$(O$^1$D) were used to constrain the model. The other photolysis rates were calculated based on a two-stream scattering model (Hough, 1988) and assuming clear-sky conditions. Under cloudy conditions calculated $J$ values were scaled to the ratio of observed $j$(O$^1$D) to clear sky $j$(O$^1$D). Dry deposition terms for H$_2$O$_2$ (1 cm s$^{-1}$) (Junkermann and Stockwell, 1999), RO$_2$H (0.9 cm s$^{-1}$) (Junkermann and Stockwell, 1999), HNO$_3$ (0.8 cm s$^{-1}$) (Ganzeveld and Lelieveld, 1995), CH$_3$OH (0.09 cm s$^{-1}$) (Carpenter et al., 2004) and HCHO and aldehydes (0.33 cm s$^{-1}$) (Brasseur et al., 1998) were included in the model. The model was constrained to hourly measurements of a number of VOCs (listed explicitly in Table 1), NO$_x$, O$_3$, CO, CH$_4$, $j$(O$^1$D) and meteorological parameters. The midday concentrations/values of these model constraints are given in Table 1 for information; there were, however, some deviations from these typical midday values in the hourly measurements that were used as model inputs. The halogen scheme was constrained using measurements of the diurnal cycle of [IO] and [BrO] averaged for May 2007. It was necessary to use an average because of incomplete data coverage primarily arising from IO and BrO being detected by DOAS in different wavelength regions and, therefore, not being measured simultaneously. A H$_2$ concentration of 500 ppbv was used, similar to that

measured in the remote MBL at other locations, for example during SOAPEX-2 at Cape Grim (Sommariva et al., 2004), and used in OH model calculations during the ALBATROSS campaign (Brauers et al., 2001). A constant HCHO concentration of 328 pptv was assumed in the base-case model scenario, based on average [HCHO] measured by LP-DOAS during May at the observatory (Mahajan et al., 2010). Deviations from this background [HCHO] used (and the impact upon HO$_x$ levels) are considered in Sect. 3.4. The unmeasured intermediate species, generated from the oxidation of VOCs and other species used to constrain the model, were initialised at zero. The simultaneous rate equations were solved using the FACSIMILE integrator (Curtis and Sweetenham, 1987). The model was allowed to run to steady state (~4 days) to stabilise the concentrations of any unmeasured intermediate species, e.g. alkyl nitrates, unmeasured carbonyls and peroxides, before the OH and HO$_2$ modelled data were compared to the measurements.

The rate of heterogeneous loss of HO$_2$ and a number of halogenated species (supplementary information: http://www.atmos-chem-phys.net/10/1555/2010/acp-10-1555-2010-supplement.pdf) to aerosol surfaces has been included in the model. A simple scheme was used, based on a first-order loss to aerosol surfaces (Ravishankara, 1997):

$$k'_{\text{loss}} = \frac{c_g A \gamma}{4} \tag{4}$$

where $c_g$ is the mean molecular speed of the gas molecules (cm s$^{-1}$), calculated using Eq. (5):

$$c_g = \sqrt{\frac{8\,RT}{\pi\,M_w}} \tag{5}$$

$k'_{\text{loss}}$ is the heterogeneous loss rate, $A$ is the aerosol surface area per unit volume, $\gamma$ is the uptake coefficient, $R$ is the universal gas constant, $T$ is temperature and $M_w$ is the molecular weight of the gas. More recently, this scheme was extended by Sommariva et al. (2006) and Haggerstone et al. (2005) to incorporate loss rates that were dependent upon the measured aerosol size-distribution, using an expression which incorporated the transition between control by gas-phase diffusion and molecular uptake (Sander, 1999). In the background marine environment, the particle diameters are small. Under such conditions, mass transfer is limited by interfacial mass transport and Eq. (4) provides a reasonable estimation of the aerosol uptake coefficient (Haggerstone et al., 2005).

The particle radius and number population, used to determine the aerosol surface area, were measured with a Scanning Mobility Particle Sizer (SMPS) (0–1 μm) and a Aerosol Particle Sizer (APS) (1–10 μm) (Allan et al., 2009) at a height of 30 m. The average aerosol surface area observed at the CVAO at this height during the project was ~1×10$^{-6}$ cm$^2$ cm$^{-3}$. For particles of 0–1 μm diameter (which encompasses the bulk of the aerosols at the site) a dry aerosol distribution was determined. At an average ambient humidity of ~80% the radius of sea-salt aerosols are expected to grow by a factor of ~1.4 (Allan et al., 2009), leading to an ambient aerosol surface area of roughly a factor of 2 (radius$^2$) larger for this size range. A strong gradient in the aerosol surface area at the ground to a height of ~12 m has recently been recorded at the site (von Glasow, 2009). It is estimated from these gradient measurements that the aerosol surface area is approximately a factor of 2 greater at the height of the FAGE nozzle (~3.5 m) compared with the aerosol surface area at 30 m. To account for the difference in sampling height and aerosol growth factors an aerosol surface area of 4×10$^{-6}$ cm$^2$ cm$^{-3}$ was used in model calculations. An uptake coefficient ($\gamma$) of 0.1 was used based on recent recommendations (Taketani et al., 2008). Sensitivity analyses have been performed on the aerosol uptake (see Sect. 3.4 for further details).

A surface deposition term for HO$_2$ was also considered. The deposition velocity ($V_D$) of HO$_2$ was estimated using the NOAA/COARE air/sea gas exchange parameterization (Fairall et al., 2007). The deposition velocity of HO$_2$ is related to the flux ($F$) of HO$_2$ at a given height above the surface ($z$) by:

$$F = -V_D \times [\text{HO}_2]_{(z)} \tag{6}$$

$V_D$ can be determined given knowledge of the sum of air-side ($R_a$) and water-side ($R_w$) resistances (Fairall et al., 2000):

$$V_D = \left( \frac{1}{R_a + (R_w/\alpha)} \right) \tag{7}$$

where $\alpha$ is the dimensionless solubility (a function of species, temperature and salinity). The air-side resistance, $R_a$, represents the sum of the aerodynamic resistance ($R_1$) and gas-phase film resistance ($R_2$). Assuming that the atmospheric surface layer is neutrally stable then $R_1$ can be determined using Eq. (8):

$$R_1 = \frac{U_{(z)}}{u_*^2} = \frac{1}{\kappa u_*} \ln\left(\frac{z}{z_0}\right) \tag{8}$$

where $U_{(z)}$ is the mean wind-speed at height ($z$), $\kappa$ is the von Karman constant (0.4), $u_*$, is the friction velocity, and $z_0$, is the aerodynamic roughness length (Stull, 1988). The gas-phase film resistance ($R_2$) is determined by Eq. (9):

$$R_2 = \frac{5}{u_*} S_C^{2/3} \tag{9}$$

where $S_C$ is the Schmidt number.

The water-side resistance ($R_w$) can be determined by Eq. (10) (assuming the influence of turbulence is negligible relative to chemical reaction time-scale of HO$_2$ in water):

$$R_w = \frac{1}{\sqrt{a D_w}} \tag{10}$$
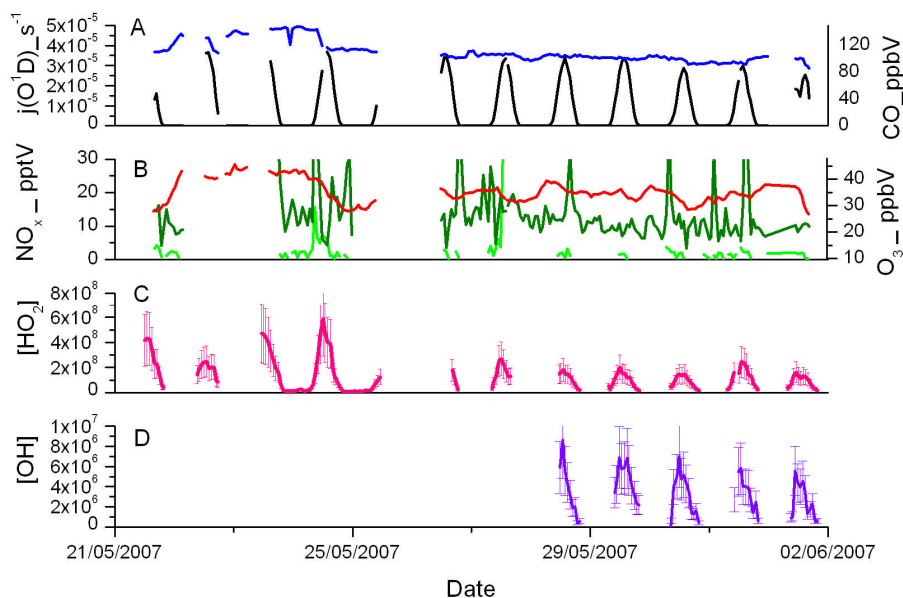
**Fig. 3.** Panel (**A**): Time-series of $j(O^1D)$ (black line) and CO (blue line) from the HO$_x$ measurement period (gaps in data are due to power failures). Panel (**B**): Time-series of NO (lime line), NO$_2$ (green line) and O$_3$ (red line) from the HO$_x$ measurement period (gaps in data are due to power failures or instrument down-time). Panel (**C**): Time-series of measured HO$_2$ in molecule cm$^{-3}$ (pink line) with the 2 $\sigma$ standard deviation shown. Panel (**D**): Time-series of measured OH in molecule cm$^{-3}$ (purple line) with the 2 $\sigma$ standard deviation shown. All data are hourly averaged.

where $a$ is the reaction time-scale for HO$_2$ in water (assumed to be sufficiently fast that turbulence is neglected) and $D_w$ is the diffusion coefficient of HO$_2$ in water.

Many of the variables in Eqs. (7)–Eq. (10) can be estimated by the NOAA/COARE algorithm given an input of boundary layer depth ($\sim$1000 m) (Read et al., 2008), atmospheric pressure ($\sim$1010 mbar), wind-speed (0–20 m s$^{-1}$), height of wind-speed data (10 m), Henry's law coefficient (1.2$\times$10$^3$ M atm$^{-1}$ (Schwartz, 1984)) and rate coefficients for reactions of HO$_2$ in water (ionisation of HO$_2$ forming O$_2^-$ and H$^+$; Bielski, 1978, and chemical reaction of HO$_2$ with O$_2^-$ forming HO$_2^-$; Bielski, 1978, were considered). The water-side Schmidt number and diffusion coefficient were assumed to be similar to those of O$_3$ (500 and 1.2$\times$10$^{-9}$ m$^2$ s$^{-1}$; Chang et al., 2004). The HO$_2$ water-side reaction rate was varied from 10$^3$–10$^5$ s$^{-1}$ to determine the sensitivity of $V_D$ to it. For HO$_2$, the solubility is sufficiently large that the deposition velocity is essentially air-side controlled and the flux is insensitive to the water side turbulence and reaction rate.

## 3 Results

Figure 3 shows the values of $j(O^1D)$, CO, NO, NO$_2$, O$_3$, HO$_2$ and OH measured at the CVAO during the summer 2007 campaign. OH measurements were made on 5 days (28 May to 2 June) and HO$_2$ on 11 days (21 May to 2 June). From 21 May–24 May, the air-mass intercepted was characterised

by elevated levels of CO ($\sim$130 ppbv); CO levels dropped to $\sim$100 ppbv during the day on 24 May and remained at this level for the remainder of the radical measurement period (Fig. 3a). Back trajectory analysis for this period indicates a switch in air-mass origin (Lee et al., 2009a). From 21–24 May, the air intercepted had originated (at a low altitude) over the western north Atlantic and continental America before being transported at a higher altitude over the ocean and descending close to the Cape Verde islands. From 26–29 May the air sampled originated over Southern Europe and the Mediterranean (usually within the boundary layer), before passing near to the Canary Islands on its way to Cape Verde. [CO] remained at background levels ($\sim$100 ppbv) between 26–29 May suggesting that this air-mass was not strongly influenced by anthropogenic emissions from Europe. From 30 May onwards, the CVAO largely sampled air that was mid north Atlantic in origin, passing close to the Canary Islands before approaching Cape Verde from a North Easterly direction. Throughout the measurement period the maximum noontime $j(O^1D)$ levels were relatively constant, at 3.5$\times$10$^{-5}$ s$^{-1}$ (Fig. 3a) with very little cloud cover observed throughout the campaign. O$_3$ concentrations between 35–40 ppbv were recorded (Fig. 3b) (Lee et al., 2009a).

### 3.1 Daytime measured and modelled OH and HO$_2$

During 3 out of the first 4 days of measurements [HO$_2$] was elevated relative to data taken later in the campaign, corresponding to the elevated CO during this time, with a
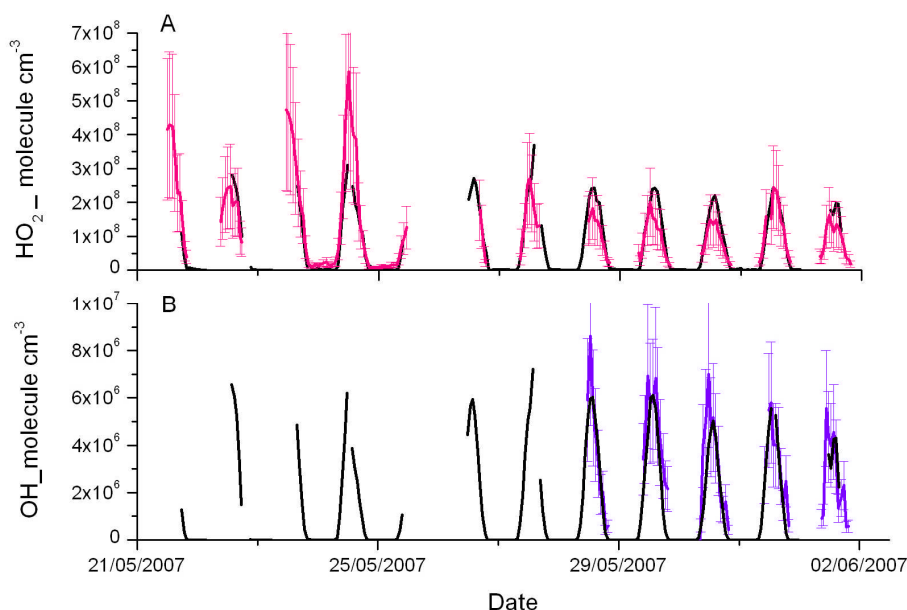
**Fig. 4.** Panel **(A)**: Time-series of measured HO$_2$ in molecule cm$^{-3}$ (pink line) with the 2 $\sigma$ standard deviation shown and MCM calculated [HO$_2$] (base-case scenario, see text for details) (black line). Panel **(B)**: Time-series of measured OH in molecule cm$^{-3}$ (purple line) with the 2 $\sigma$ standard deviation shown, and MCM [OH] calculated (base-case scenario, see text for details) (black line). All data represent a 1 h average.

maximum of $\sim$6$\times$10$^8$ molecule cm$^{-3}$ ($\sim$24.5 pptv) recorded on 24 May (Fig. 3c); [NO$_x$] were elevated on this day and may indicate a local pollution source. MCM model estimates of [HO$_2$] over this period are also elevated relative to model estimates for later in the campaign (Fig. 4a), although peak MCM modelled [HO$_2$] from this period is only $\sim$3$\times$10$^8$ molecule cm$^{-3}$, suggesting either a missing source of HO$_2$, or an over-estimation of the HO$_2$ sinks in the model; the modelled [HO$_2$] estimates are $\sim$39% lower than those measured during this phase (falling outside the 1 $\sigma$ measurement uncertainty). The daily variability observed in [HO$_2$] during this period is also not captured by the model; on 22 May, measured [HO$_2$] was significantly lower at $\sim$3$\times$10$^8$ molecule cm$^{-3}$, but this drop in [HO$_2$] was not reflected in the model. The lack of variability in the modelled HO$_2$ may be due, in part, to the use of a constant average diurnal cycle for IO and BrO, constant heterogeneous losses and/or constant [HCHO]. Sensitivity analyses of [HO$_2$] to each of these modelled parameters have been performed and are presented in Sect. 3.4.

After 26 May the peak measured [HO$_2$] were lower $\sim$2–4$\times$10$^8$ molecule cm$^{-3}$, and are mirrored by the model. The model is in much better agreement with [HO$_2$] measurements during this phase, overestimating [HO$_2$] by 16% on average; this is within the 1 $\sigma$ measurement uncertainty of 20%.

OH measurements were also made during the second measurement period (Fig. 3c). Peak concentrations of 6–9$\times$10$^6$ molecule cm$^{-3}$ were recorded; the midday [OH] gradually decreasing over the 5 days. The model

under-predicted [OH] on average by 18%, although again this is within the 1 $\sigma$ measurement uncertainty.

## 3.2 Nighttime measured and modelled HO$_2$

Low concentrations ($\sim$0.6 pptv) of HO$_2$ were measured on two nights (24 and 25 May); due to the instrumental difficulties, outlined in Sect. 2.1 no nightime OH measurements were made. Model estimates of nighttime HO$_2$ significantly under-predict the observations, however (Fig. 5). As reported by Read et al. (2008) a daily O$_3$ destruction cycle is observable at the CVAO, with the majority of this loss due to photolysis of O$_3$ and subsequent reaction of O($^1$D) with H$_2$O vapour and via catalytic cycles involving IO and BrO. The O$_3$ concentration is replenished during the night by entrainment of air from the free tropopshere that is richer in O$_3$, followed by advection to the site (Read et al., 2008). The HO$_2$ concentration was observed to decrease to a minimum at $\sim$21:30 and then slowly increase throughout the remainder of the night, analogous to the observed nighttime O$_3$ profile, suggesting that the entrained air during the night is providing a source of radicals.

The nighttime generation of OH and HO$_2$ in the MCM box model is from reactions of O$_3$ with alkenes, specifically propene ($\sim$72%) and isoprene and its oxidation products ($\sim$25%). The reaction of NO$_3$ with alkenes is not a significant source of HO$_2$, unlike Mace Head (Salisbury et al., 2001). The OH generated from O$_3$ + alkene reactions reacts with acetaldehyde and methane, leading to the formation of
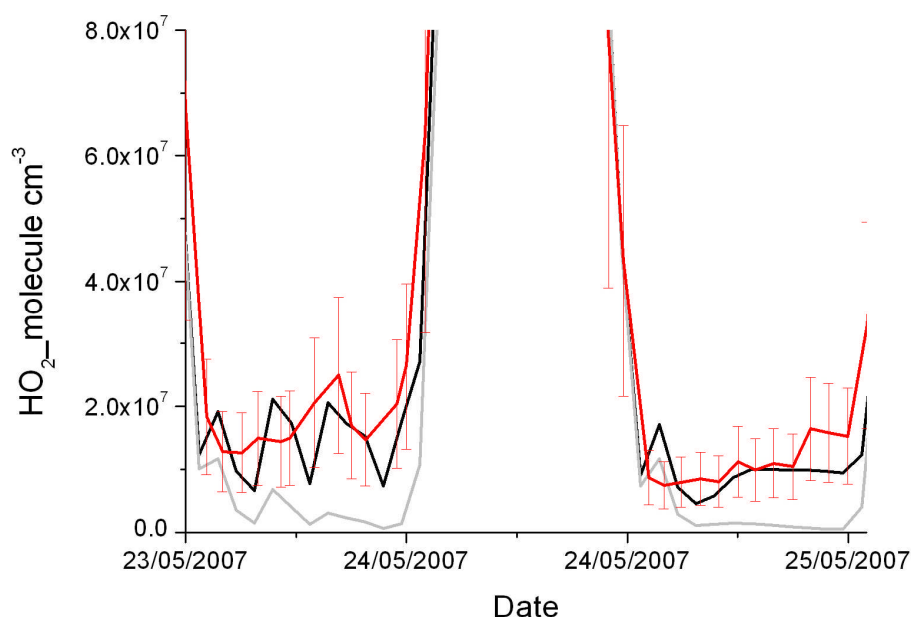
**Fig. 5.** Time-series of nighttime [HO$_2$] measured on two consecutive nights. The red line represents the measured HO$_2$, with the 2 $\sigma$ standard deviation shown. The grey and black lines represent modelled [HO$_2$] when the model is left unconstrained to PAN and when [PAN] is held at 100 pptv respectively.

peroxy radicals, which in turn, through self reaction or reaction with NO generate HO$_2$. Alternatively, OH reacts with CO, generating HO$_2$ directly. The OH and HO$_2$ radicals are strongly coupled at night with $\sim$37% of OH formed from the O$_3$+HO$_2$ reaction. The model underestimation of HO$_2$ at night may derive from an unmeasured alkene, possibly one that is biogenic in origin. Phytoplankton in oceans are known to produce a large suite of VOCs (Moore et al., 1994; Shaw et al., 2003). It is likely, however, that this source would also be present in the daytime, and so would have to be included as an OH sink.

The entrainment of peroxyacetyl nitrate (PAN) may also act as a nighttime (as well as daytime) source of radicals. In the modelling presented thus far, PAN is unconstrained in the model, and the modelled concentration peaks at $\sim$100 pptv at $\sim$15:00, corresponding to the peak in NO$_2$ and then decreases to $\sim$10 pptv during the night. The thermal decomposition lifetime of PAN is just 20 min at 300 K (Bridier et al., 1991), and entrainment of air from the cooler free troposphere (where the PAN lifetime will be much longer) could lead to the rapid decomposition of the molecule, leading to an additional source of radicals. To test this hypothesis, the PAN concentration was constrained in the model to a constant 100 pptv (during both the day and night). Running the model with constrained PAN improves the modelled to measured HO$_2$ throughout the day and night (Fig. 5). Jacobi et al. (1999) have reported PAN concentrations measured during a cruise of the R/V Polarstern from Cape Town (South Africa) to Bremerhaven (Gemany) in May/June 1998.

Whilst cruising a maximum of 500 km west of the African coast, corresponding to 20° W–15° E, (CVAO is $\sim$500 km west of the coast) PAN concentrations north of 10° N (CVAO is at 16° 51′49) only dropped below 100 pptv on two days. In contrast to these findings, Gallagher et al. (1990) found that between 7° N–64° N and 20° W–50° W in late summer that PAN concentrations in the north Atlantic ranged from <1 pptv–40 pptv. Similarly, Muller and Rudolph (1992) did not measure PAN above the LOD of 10 pptv in the tropics (30° N–30° S) when crusising at 30° W. The proximity of the measurement sites to the African coast seems to strongly influence the PAN content of the sampled air-masses (Jacobi et al., 1999). Trajectory analysis from the RHaMBLe campaign indicated that for 21–25 May (during which time the nighttime measurements of HO$_2$ were made) the air-masses intercepted at the CVAO were influenced by the US continent. In such air-masses the PAN content may have been enhanced, and, therefore, could act as an important radical source. Measurements of PAN at the site are necessary to confirm this hypothesis.

### 3.3 Rate of production and destruction analysis

Figure 6 shows the instantaneous rates of production (ROPA) and rates of destruction analyses (RODA) for OH and HO$_2$ at solar noon (averaged for the period 12:00–13:00 LT – local time) as determined by the MCM. The ROPA and RODA are averaged over all days for which there are respective measurements of OH and HO$_2$. Figure 7 shows the diurnal
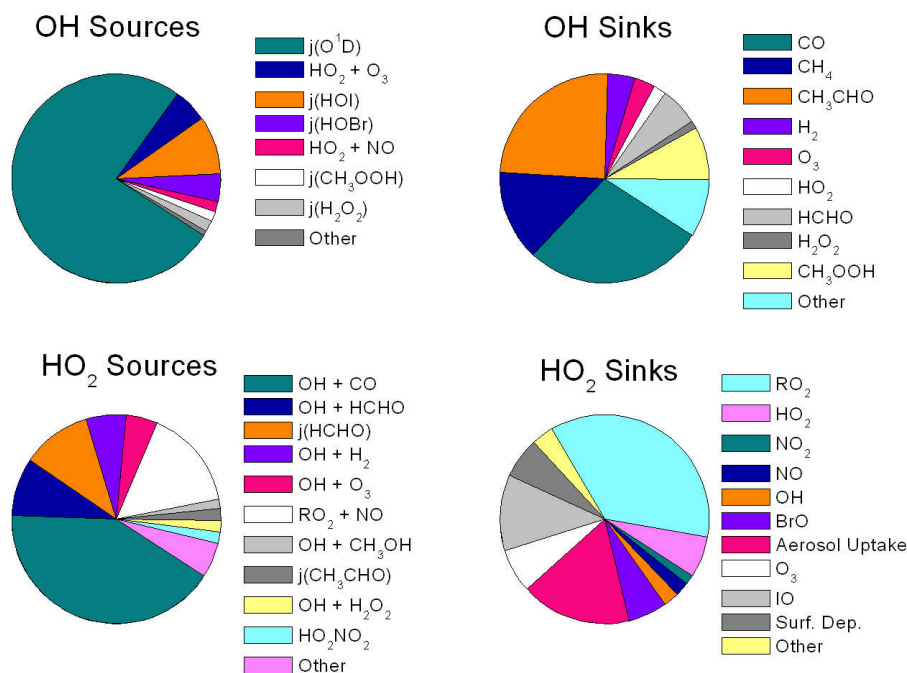
**Fig. 6.** Pie-charts showing the MCM (base-case scenario, see text for details) average diurnal modelled OH and HO$_2$ sources and sinks between 12:00–13:00.

variation of the MCM calculated rates of production and destuction of OH and HO$_2$ for different chemical processes, again averaged over the days when there are radical measurements. It should be noted that several of the pathways serve to inter-convert OH to HO$_2$, or vice versa, and so, overall, do not lead to an increase or decrease in the total HO$_x$.

The photolysis of O$_3$ and subsequent reaction with H$_2$O vapour represents the dominant OH source, accounting for ∼76% of its production at solar noon. The photolysis of H$_2$O$_2$ and CH$_3$OOH are much smaller OH sources (∼3% combined); at steady state these peroxides reach levels of ∼500 pptv and ∼1 ppbv respectively in the model, similar in magnitude to observations of peroxides at Cape Grim (Ayers et al., 1996; Monks et al., 1998) and also in the Cape Verde region during the ALBATROSS cruise (Weller et al., 2000). The recycling of HO$_2$ to OH, via reaction with NO and O$_3$, also act as small additional OH sources. The hypohalous acids, HOI and HOBr, which are generated by the reaction of HO$_2$ with IO and BrO respectively (Fig. 1), may be photolysed to OH or taken up on aerosol surfaces. An uptake coefficient for HOI and HOBr loss onto aerosols of $\gamma_{HOX}$=0.061 was assumed, consistent with experimental data (Mossinger and Cox, 2001). Under this scenario, the photolysis of HOI and HOBr contributes ∼13% to the instantaneous OH formation. There is some uncertainty in the $\gamma_{HOX}$ assumed, with some studies speculating that it may be an order of magnitude higher in the MBL (Abbatt and Waschewsky, 1998; Wachsmuth et al., 2002). The sensitivity of the modelled [OH] to this parameter is investigated in Sect. 3.4.2.

The reactions of OH with CO and acetaldehyde are the major OH losses (∼28% and ∼25% respectively). The source of acetaldehyde at remote marine locations, such as Cape Verde, has not been determined conclusively and remains subject to debate. Acetaldehyde is formed by the oxidation of primary hydrocarbons, it may derive from direct terrestrial emissions or from the photochemical degradation of organic matter in the oceans (Singh et al., 2001 and references therein). Singh et al. (2003) have inferred from aircraft measurements of acetaldehyde that the surface waters of the Pacific are greatly supersaturated with acetaldehyde and may act as a large oceanic source. Read et al. (2010) suggest that an oceanic flux of acetaldehyde is a likely source of the observed acetaldehyde concentrations in the Cape Verde region also. In contrast to acetaldehyde, the other oxygenated VOCs that were measured (acetone and methanol) play only a minor role as an OH sink (contained within "other" in Fig. 6). Other sinks include reaction with methane, H$_2$, O$_3$, HO$_2$, HCHO and peroxides. Reaction of OH with NO$_2$, C$_2$–C$_5$ hydrocarbons (NMHC) and MCM calculated chemical intermediates from OH oxidation of NMHC (oxygenated VOCs and organo-nitrates) all account for a small fraction of the OH loss, and are contained within the "other" segment also.

HO$_2$ sources are dominated by the reaction of OH with CO (∼41%) and, to a smaller extent, CH$_3$O with O$_2$ (∼16%); the source of CH$_3$O is the reaction of CH$_3$O$_2$ with NO. The presence of a small quantity of NO (∼1.5 pptv) at the site serves to slightly enhance HO$_2$ levels overall, because although HO$_2$+NO removes HO$_2$
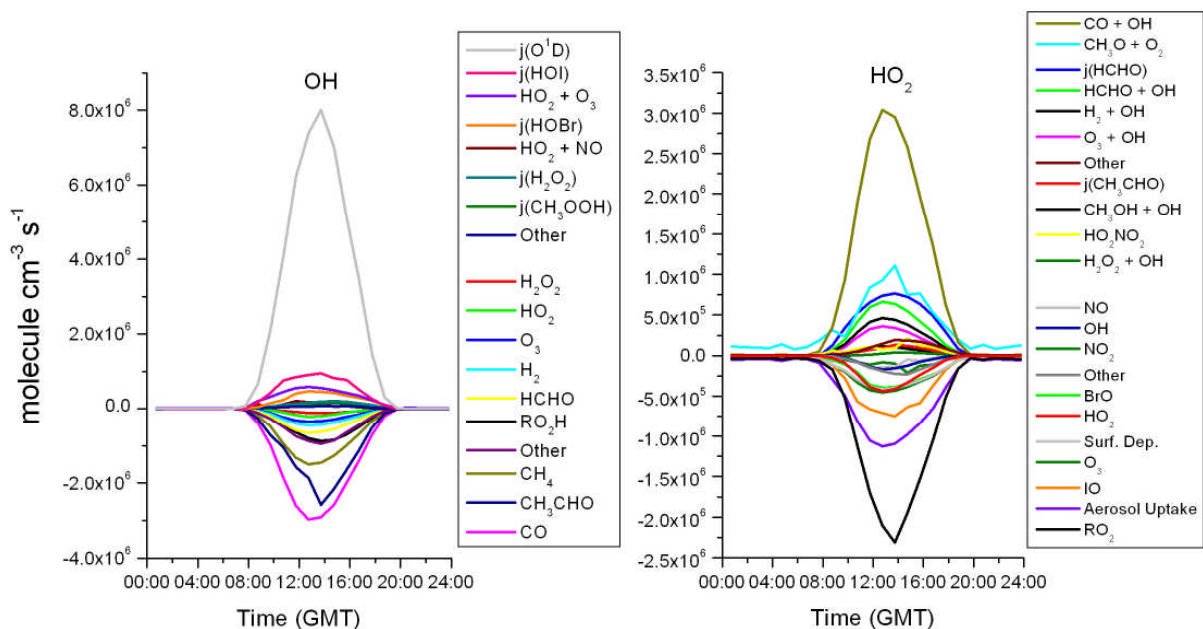
**Fig. 7.** Left: Diurnal variation of the rate of OH production and loss calculated using the MCM. Right: Diurnal variation of the rate of HO$_2$ production and loss taken from the MCM (base case, see text for details).

(Reaction R10), this is offset at these low levels of [NO] by a larger overall rate of RO$_2$+NO $\rightarrow$ RO+NO$_2$ (followed by rapid HO$_2$ production from RO+O$_2$) leading to a net production of HO$_2$ (Reactions R11 and R14) (Poppe, 1999). If NO concentrations were to increase further, [RO$_2$] would decrease (Fleming et al., 2006) and HO$_2$+NO (Reaction R10) would begin to dominate over RO$_2$+NO (Reaction R11) (as $k_{10}$=8.9×10$^{-12}$ molecule$^{-1}$ cm$^3$ s$^{-1}$ is >$k_{11}$=7.7×10$^{-12}$ molecule$^{-1}$ cm$^3$ s$^{-1}$ (IUPAC, 2006)). Under this regime, reactions involving NO would act as an HO$_2$ sink rather than a source. The sensitivity of the radicals to NO$_x$ levels is further discussed in the subsequent section (Sect. 3.4.2).

$$RO + O_2 \rightarrow Aldehyde + HO_2 \qquad (R14)$$
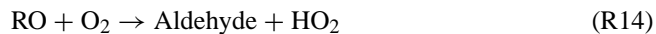
The reaction of HCHO with OH, combined with the photolysis of HCHO, can contribute close to 20% of the HO$_2$ at solar noon. Other smaller HO$_2$ sources include OH+H$_2$, OH+O$_3$, CH$_3$OH+OH, $j$(CH$_3$CHO), OH+H$_2$O$_2$ and HO$_2$NO$_2$ thermolysis.

The reaction of HO$_2$ with IO and BrO accounts for a combined, instantaneous, HO$_2$ loss of ~19%, despite these species only being present at ~1.4 pptv and ~2.5 pptv (peak daytime levels) respectively. The major HO$_2$ sink is the reaction with RO$_2$ (R=CH$_3$–C$_5$H$_{11}$) (Reaction R15), typical of low NO$_x$ environments (Carpenter et al., 1997; Penkett et al., 1997), which together with the self reaction (Reaction R16) accounts for over 40% of the total HO$_2$ loss.

$$HO_2 + RO_2 \rightarrow RO_2H + O_2 \qquad (R15)$$

$$HO_2 + HO_2 \rightarrow H_2O_2 + O_2 \qquad (R16)$$
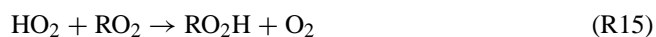
Heterogeneous loss to aerosol and surface deposition accounts for ~23% of the HO$_2$ loss at noon-time.

Over a 24 h period, the relative contribution of the HO$_x$ sources and sinks remains fairly consistent, as shown in Fig. 7. There is some deviation from the trend discussed above, and displayed in Fig. 6, for example the reaction of OH with CH$_3$CHO and reactions involving HO$_2$NO$_2$ peak in the afternoon, reflecting the afternoon peak in the concentrations of CH$_3$CHO and NO$_2$ as measured at the site. In the morning and evening (when the concentration of HO$_2$ is low) the reaction of HO$_2$ with O$_3$ dominates over the HO$_2$ self reaction promoting radical recycling rather than radical termination. The reaction of HO$_2$ with IO and BrO exhibits a broad diurnal cycle that reflects light intensity.

## 3.4 Sensitivity analysis of modelled OH and HO$_2$ concentrations

The mean diurnal profiles of the observed and modelled [OH] and [HO$_2$] has been calculated (Fig. 8) over all days for which there were respective measurements of OH and HO$_2$. Owing to instrumental difficulties outlined in Sect. 2 only daytime OH data are available. In general good agreement between the modelled and measured [OH] profile is achieved (Fig. 8a and C). The model under-predicts [OH] in the mid-morning, and during the very late afternoon and evening, although for the latter, OH levels are close to the LOD of the instrument. HO$_2$ was measured on 11 days and
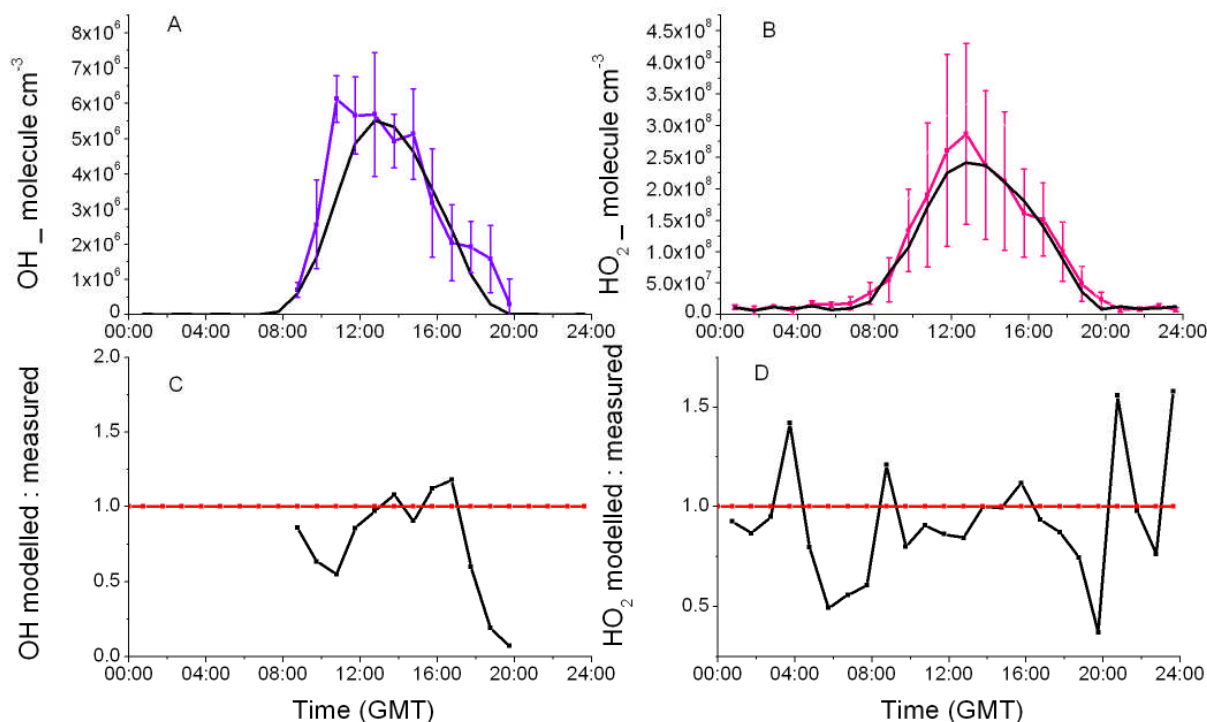
**Fig. 8.** Panel **(A)**: Average diurnal [OH] calculated for the 5 days of measurements (data on an hourly time-scale); the error bars represent the standard deviation of the data that were averaged (purple points and line). The modelled average diurnal (averaged over the 5 days of OH measurements) is also shown (MCM= grey line). Panel **(B)**: Average diurnal [HO$_2$] calculated for the 11 days of measurements (data on an hourly time-scale; the error bars represent the standard deviation of the data that was averaged (pink points and line). The modelled average diurnal (averaged over the 11 days of HO$_2$ measurements) is also shown (MCM= black line). Panel **(C)**: Solid line, with black squares represents the (OH MCM modelled)/(OH measured) ratio averaged for 1 h over 24 h. Panel **(D)**: Solid line represents the (HO$_2$ MCM modelled)/(HO$_2$ measured ratio) averaged for 1 h, for a 24 h period. Red line in panels C and D represents modelled : measured ratio of 1.

2 nights, enabling a complete 24 h average diurnal profile to be built up. Excellent agreement between observed and modelled [HO$_2$] is achieved (Fig. 8b and d) during the daytime; during the nightime the [HO$_2$] is replicated when the model is constrained to a constant [PAN] of 100 pptv (Sect. 3.2). As highlighted in Figs. 3 and 4 (and discussed in Sect. 3.1), significant variability was observed in the measured daily peak [HO$_2$], certainly when different air-masses were intercepted; this variability was not replicated in model simulations to the same extent and so the agreement between the modelled and measured [HO$_2$] in Fig. 8 may be slightly fortuitous. It should be noted, however, that owing to the more extensive data coverage during the latter half of the measurement period, when the agreement between the daily modelled and observed [HO$_2$] was at its best (Fig. 4), the diurnal profiles will be more heavily weighted to this phase. Several key modelled parameters that control the production and loss of HO$_2$ have been identified in Sect. 3.3, a number of which were either held at constant values ([HCHO] and heterogeneous chemistry) or used a constant diurnal profile ([XO]) within the model. A number of model scenarios in which these parameters are varied have been run to

determine the impact of these on the modelled [HO$_2$] (and [OH]) and to assess whether varying these parameters could account for the daily variability in the observations. Table 2 lists the changes made and their impact on modelled [HO$_2$], and Fig. 9 shows the impact on the diurnal variation of the modelled-to-measured ratio of [HO$_2$]. The uptake coefficient of the hypohalous acids has also been varied, in accord with reported literature values, to determine the sensitivity of [OH] (and [HO$_2$]) to this:

### 3.4.1 HCHO

As discussed in Sect. 3.3, the reaction of OH with HCHO and HCHO photolysis are sources of HO$_2$. The model thus far has been constrained to a constant HCHO concentration of 328 pptv, which is the mean HCHO concentration observed during May 2007, as measured using the LP-DOAS during its 8 month deployment at the observatory. It should be noted, however, that throughout the 8 months [HCHO] were variable, dropping below the LOD of the LP-DOAS (~200 pptv) at times and elevated in polluted air-masses. Recent analysis of the HCHO data during the RHaMBLe measurement intensive has highlighted that [HCHO] were

**Table 2.** List of parameters that have been varied to optimise the HO₂ modelled to measured agreement. The daytime % change was averaged from 08:44–19:44; the nighttime % change was averaged from 19:44–08:44.

| Model Parameter | Parameter Change | Av. % Change in HO₂ (day) | Av. % Change in HO₂ (night) | Av. % Change in OH (day) |
|---|---|---|---|---|
| HCHO | 328 pptv → 100 pptv | −8 | 0 | +2 |
| HCHO | 328 pptv → 2000 pptv | +60 | +1 | −9 |
| Halogen chemistry | XO chemistry switched off | +12 | +2 | −12 |
| Halogen chemistry (modified [NO$_x$] | XO chemistry switched off & [NO$_x$] → doubled | +18 | 0 | −9 |
| Hypohalous acid chemistry | $\gamma_{HOX}$=0.061 → 0.61 | −2 | 0 | −4 |
| Aerosol uptake | Included → Not included | +29 | +59 | +7 |
| Surface deposition | Included → Not included | +9 | +16 | +2 |
| Heterogeneous losses & halogen chemistry | No heterogeneous loss, no IO chemistry, [BrO]×1.4 | +52 | +104 | −3 |
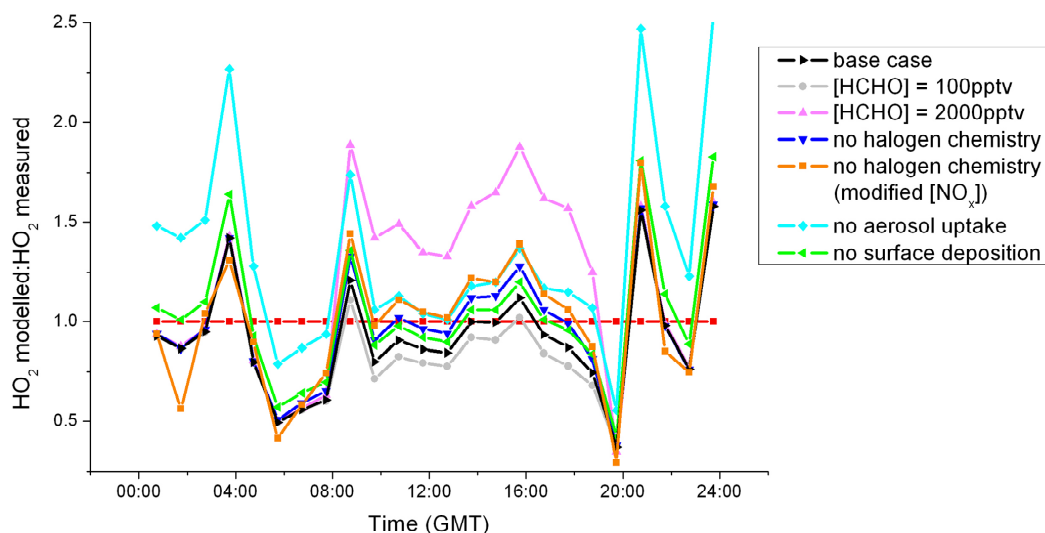


**Fig. 9.** (HO₂ MCM modelled)/(HO₂ measured) ratio for a number of different model scenarios. Black line = base case scenario (with [PAN]= 100 pptv) , all other scenarios are based on this model with the specified (see legend) parameters adjusted. Red line represents an (HO₂ MCM modelled)/(HO₂ measured) of 1. See text and Table 2 for further details.

extremely elevated (∼2 ppbv) on the 23 and 24 May (and also on the 27 and 28 May, although HO₂ data is limited during this second period due to power cuts). These large excursions from the more typical [HCHO] used in the model could account for the model's failure to replicate the elevated [HO₂] observed at the beginning of the measurement period (Fig. 4).

Two model runs whereby [HCHO] was reduced to 100 pptv (Fig. 9, grey line) and increased to 2 ppbv (Fig. 9, pink line) have been performed. Reducing the HCHO concentration from 328 pptv to 100 pptv decreases [HO₂] by ∼8% during the daytime, but does not effect the night-time levels of HO₂ (Table 2); at [HCHO] of 2 ppbv, [HO₂]

increases by ∼60% on average from the base-case scenario. Approximately a 140% increase in the base-case model is required to match the elevated [HO₂] observed at the beginning of the measurement period. This remaining discrepancy may indicate that the model is missing other additional HO₂ sources at this time or potentially that the HO₂ sinks are over-estimated by the model at this time (see Sect. 3.4.2 and 3.4.3). During the ALBATROSS cruise, up to 1 ppbv of HCHO was observed in the tropical mid-Atlantic (Brauers et al., 2001) and ∼750 pptv was recorded in the Cape Verde region (Weller et al., 2000). At Cape Grim, Tasmania during the SOAPEX-2 campaign, during clean conditions, [HCHO] was measured around noon from 217–352 pptv (with 50%

error) (Sommariva et al., 2004). The source of the high [HCHO] observed during RHaMBLe may be caused by long-range transport of polluted air from America; this will be further investigated in future publications (Mahajan et al., 2010).

### 3.4.2 Halogen chemistry

The inclusion of a halogen scheme has been shown to improve the HO$_2$ modelled to measured agreement at a number of marine locations (Bloss et al., 2005b; Smith et al., 2006; Sommariva et al., 2006; Kanaya et al., 2007). Sommariva et al. (2006) report that combined, IO and BrO accounted for ~30% of the HO$_2$ loss term during the NAMBLEX campaign at [IO]=4 pptv and [BrO]=6.5 pptv. Switching the halogen chemistry off in the Cape Verde model serves to increase [HO$_2$] by ~12% during the daytime and ~2% during the night. [OH] decreases by ~12%. Sommariva et al. (2006) found that the modelled to measured HO$_2$ agreement could be improved further during the NAMBLEX campaign by making the assumption that the source of IO was not evenly distributed over the DOAS light-path, rather it was concentrated by the shore close to the HO$_2$ FAGE measurements, and as a consequence [IO] was ~10 times higher by the FAGE inlet. There are no macro-algae beds around the Cape Verde islands unlike Mace Head that could be acting as a source of IO and so it is unlikely that there is a hotspot of IO production by the CVAO; this is supported by the good modelled to measured HO$_2$ agreement that exists when it is assumed that the [IO] is evenly distributed throughout the DOAS lightpath, representative of an oceanic source. If there were some variability in the oceanic emissions from day to day this could account for some of the variability observed in the HO$_2$ concentrations.

As discussed in Sect. 3.3, the overall impact of halogen chemistry on the OH concentration will be dependent upon the uptake coefficient assumed for the hypohalous acid species. To investigate the sensitivity of [OH] and [HO$_2$] to this parameter, a model run was performed in which $\gamma_{HOX}$ was increased 10 fold from the base-case run (see Table 2). The [OH] was found to decrease by 4% during the day and so under this scenario the impact of halogen oxides upon [OH] and on the oxidising capacity is reduced, although the photolysis of HOI and HOBr is still acting as a significant OH source. The [HO$_2$] during the daytime is also reduced by 2% under this scenario as a consequence of the reduction in the rate of reaction of OH with CO.

The presence of halogen oxides not only serves to modify the HO$_x$ chemistry, but also the NO$_x$ chemistry by accelerating NO$_x$ oxidation through Reactions (R7) and (R17). Thus far, the impact of IO and BrO on NO$_x$ chemistry has not been considered, yet any change in the NO:NO$_2$ ratio can perturb the OH:HO$_2$ ratio by changing the rate of Reactions (R10) and (R11).

$$XO + NO_2 + M \rightarrow XONO_2 + M \qquad (R17)$$
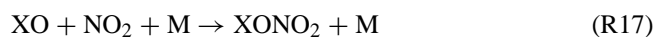
Keene et al. (2009) report a reduction in [OH] in a modelling study when halogen oxide chemistry was included as a consequence in the reduction in the secondary formation of OH via Reaction R10 (Keene et al., 2009). Modelling studies indicate that NO$_x$ levels could approximately double in the absence of halogen oxides in environments similar to Cape Verde (Keene et al., 2009). To simulate the overall impact of halogen oxides, taking into account that NO$_x$ levels may be significantly perturbed due to the presence of halogens, a model run, initialised with no halogens and a factor of two increase in the NO$_x$ concentration, has been performed. In contrast to Keene et al. (2009), OH concentrations were found to be 9% larger in the presence of halogen oxides compared to in the absence of halogen oxides (but with double [NO$_x$]) (Table 2); the perturbation of the NO$_x$ chemistry by halogen oxides offsets the instantaneous OH formation via HOI and HOBr photolysis by ~3%. Keene et al. (2009) consider the impact of BrO and ClO only; no IO measurements were made. The rate coefficient for reaction of ClO with HO$_2$ ($5 \times 10^{-12}$ molecule$^{-1}$ cm$^3$ s$^{-1}$; IUPAC, 2006) is a factor of two times smaller than the rate coefficient for reaction of ClO with NO ($1.7 \times 10^{-11}$ molecule$^{-1}$ cm$^3$ s$^{-1}$; IUPAC, 2006). Depending on [HO$_2$] and [NO], the presence of ClO can effectively lead to a reduction in [OH], as presented by Keene et al. (2009). Conversely, the rate coefficient for reaction of IO with HO$_2$ ($8.4 \times 10^{-11}$ molecule$^{-1}$ cm$^3$ s$^{-1}$; IUPAC, 2006) is larger than the rate coefficient for reaction of IO with NO ($1.96 \times 10^{-11}$ molecule$^{-1}$ cm$^3$ s$^{-1}$; IUPAC, 2006) and so the presence of IO, in low NO$_x$ environments, serves to increase [OH]. The absence of IO chemistry in the model used by Keene et al. (2009) could account for the differences in the modelled impacts of halogens on [OH]. The difference between the two model scenerios in which halogen chemistry is switched off and NO$_x$ chemistry is (a) constrained to observations and (b) is doubled, allows the impact of variable [NO$_x$] upon [OH] and [HO$_2$] to be assessed. On average, modelled [OH] and [HO$_2$] increased by a further 3% and 6% respectively via increases in Reactions (R10) and (R11) when [NO$_x$] was set to twice the observations. As discussed above, halogen oxides can perturb this chemistry and need to be condsidered alongside NO$_x$ to predict how potential changes in [NO$_x$] may impact [HO$_x$] in this environment.

### 3.4.3 Heterogeneous losses of HO$_2$

Heterogeneous loss of HO$_2$ acts as a large HO$_2$ sink (Sect. 3.3). If the uptake onto aerosol surfaces is assumed negligible, modelled [HO$_2$] increases by 29% during the daytime and by 59% at night, leading to a large modelled HO$_2$ over-prediction. A change in the aerosol surface area and/or composition could account for some of the daily variability observed in HO$_2$. Thornton et al. (2008) report that the uptake coefficient for HO$_2$ may vary considerably with changes in aerosol composition. Certainly, if heterogenous
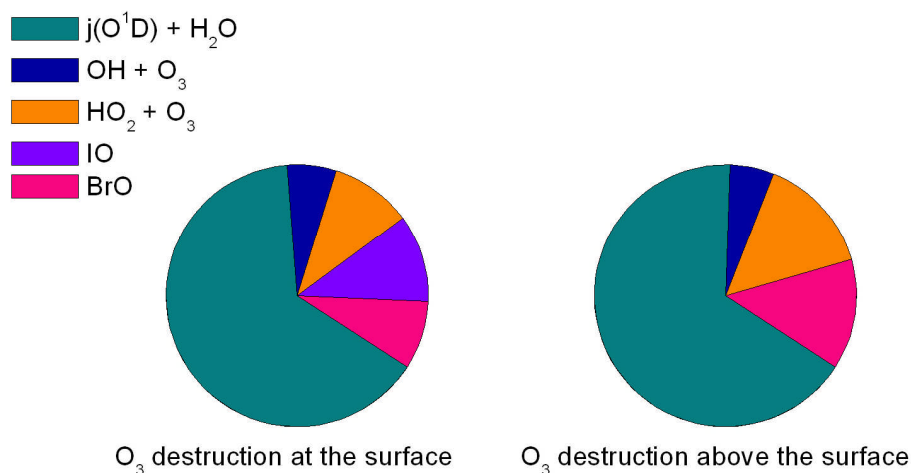
**Fig. 10.** Pie-charts highlighting the key parameters that cause the daily $O_3$ destruction that is observed at the CVAO both at the surface (left panel) and at the top of the MBL (right panel). Total $O_3$ destruction calculated using 12 h averaged, daytime, data was ∼4 ppbv at the surface and ∼3.5 ppbv at the top of the MBL.

loss processes to aerosol surfaces were lower during the interception of the long-range transported airmass compared with loss processes during the interception of tropical Atlantic marine air then this (combined with elevated [HCHO]) may account for the model under-prediction of [HO₂] at the beginning of the campaign. Furthermore, the sensitivity of modelled [HO₂] to aerosol uptake, coupled with the steep gradient in aerosol surface area from the ground to a height of 30 m (Sect. 2.3) suggests that [HO₂] could vary significantly with altitude within the BL.

In addition to heterogeneous loss to aerosols, surface deposition of HO₂ to the surrounding ocean also contributes to the total HO₂ sink within the model, albeit to a smaller extent, and may also promote variability in [HO₂] with altitude. Without a surface deposition term, modelled [HO₂] is ∼9% higher during the daytime and ∼16% at night. Prior to reaching the FAGE cell, the sampled air passed over ∼50 m of surf zone and rocks, in addition to the open ocean, and as this area is likely to have an increased surface roughness, leading to higher turbulence and hence contact with the ground, the surface deposition assuming loss to the ocean only is likely a lower limit for this region. The uncertainties in the magnitude of the surface deposition term could affect the overall magnitude of the modelled [HO₂], but are unlikely to account for the daily variablility in the measurements at the ground.

## 4 Discussion and implications for MBL photochemistry

Tropospheric $O_3$ is an important greenhouse gas, providing a similar radiative forcing to methane, and ∼25% of that due to $CO_2$ (Forster et al., 2007), and in the troposphere forms via the catalytic oxidation of CO, methane and other VOCs in the presence of $NO_x$. $O_3$ production predominantly occurs

in continental regions where $NO_x$ is elevated, whereas in the remote tropical marine boundary layer $O_3$ is destroyed primarily through photolysis and subsequent reaction of the excited state oxygen atom with $H_2O$ vapour (Read et al., 2008). During the RHaMBLe project at the CVAO, a daily $O_3$ loss was observed of the order of ∼3.5 ppbv d$^{-1}$. Taking the daytime average concentrations for the relevant measured species from the period 21 May–2 June 2007, the relative contributions to the observed chemical loss were calculated (concentration × rate coefficient), as shown in Table 3 and Fig. 10. The photolysis of $O_3$ and subsequent reaction with $H_2O$ (Reactions R1 and R2) accounts for ∼40% of the daily $O_3$ destruction. The reaction of $O_3$ with OH (9%) (Reaction R3) and HO₂ (12%) (Reaction R4) also contributes to its loss, owing to the relatively high concentrations of the radicals at the site, and reaction with IO (22.5%) and BrO (16.5%) also destroy $O_3$ (Reactions R5–R9). Table 3 highlights the relative importance of the reactions which contribute to the chemical destruction of $O_3$. When combined, BrO and IO together destroy ∼1.5 ppbv d$^{-1}$, whilst the loss due to the combined reaction with OH and HO₂ is just under 1 ppbv d$^{-1}$, in good agreement with estimates reported by Read et al. (2008) for the month of May. Read et al. (2008), however, used a box model to calculate OH and HO₂ for the purposes of calculating the rate of $O_3$ destruction, rather than using the measured values directly in the field, as presented here.

Aircraft measurements of $O_3$ made above the CVAO during the RHaMBLe project (Read et al., 2008) demonstrated that the $O_3$ destruction observed at ground level occurs throughout the entire MBL, which typically extends to ∼1 km altitude. The IO and BrO, observed by the LP-DOAS at the site, originate from the photolysis of organo-iodine compounds volatilised from the ocean and the acid-catalysed

**Table 3.** The rates of the rate-limiting O$_3$ destruction steps and their percentage contribution towards O$_3$ destruction both in the surface layer and at the top of the MBL (1 km), see text for details.

| O$_3$ destruction rate determining step | Contribution to O$_3$ destruction at the surface (molecule cm$^{-3}$ s$^{-1}$) | Contribution to O$_3$ destruction at the top of the BL (molecule cm$^{-3}$ s$^{-1}$) |
|---|---|---|
| O$^1$D+H$_2$O | $9 \times 10^5$ (40%) | $9 \times 10^5$ (45%) |
| OH+O$_3$ | $2.1 \times 10^5$ (9%) | $2 \times 10^5$ (9%) |
| HO$_2$+O$_3$ | $2.6 \times 10^5$ (12%) | $3.8 \times 10^5$ (18%) |
| IO+IO | $7.2 \times 10^4$ (3%) | 0% |
| IO+HO$_2$ | $3.6 \times 10^5$ (16%) | 0% |
| IO+NO | $2.7 \times 10^4$ (1%) | 0% |
| IO+BrO | $1.1 \times 10^5$ (5%) | 0% |
| BrO+BrO | $1.4 \times 10^4$ (1%) | $2.7 \times 10^4$ (1%) |
| BrO+HO$_2$ | $2.1 \times 10^5$ (10%) | $4.5 \times 10^5$ (22%) |
| BrO+NO | $6.7 \times 10^4$ (3%) | $9.4 \times 10^4$ (5%) |
| Total | $2.2 \times 10^6$ (3.91 ppbv d$^{-1}$) | $2.0 \times 10^6$ (3.59 ppbv d$^{-1}$) |

activation of bromine from sea-salt aerosols, respectively (Read et al., 2008). There is some evidence to suggest that [BrO] may increase with altitude in the MBL (von Glasow et al., 2002) owing to an increase in the acidity of sea salt aerosols with altitude which enables acid catalysed bromine activation to occur more efficiently (von Glasow and Sander, 2001). It is uncertain, given the surface source of organo-iodine compounds and the short atmospheric lifetime of IO ($\sim$50 s), whether this molecule also prevails throughout the MBL. The rate of heterogeneous loss of HO$_2$ by uptake to aerosol surfaces and by surface deposition to the ocean (and/or rocky foreshore) will be at a maximum at ground level. The HO$_2$ measurements were made just 3.5 m a.s.l. and, as discussed above, heterogeneous losses could reduce [HO$_2$] at the ground by $\sim$38% during the daytime. As a consequence of this, the HO$_2$ concentration could increase with altitude in the boundary layer, and hence the rate of destruction of O$_3$ by the HO$_2$+O$_3$ reaction will also increase with altitude. Further increases in [HO$_2$] with height may be expected as a consequence of a reduction in the [IO] with height.

A model scenario in which [IO], and heterogenous losses are set to zero and [BrO] is increased by a factor of 1.4 to simulate chemistry at the top of the MBL predicts that [HO$_2$] could be 52% higher than at the surface during the daytime (Table 2). Table 3 and Fig. 10, right panel, highlight the impact these changing parameters may have upon O$_3$ destruction. A reduction in temperature ($\sim$5° C) is also considered as this has a small effect on the rate coefficients used. An O$_3$ loss rate of $\sim$3.91 ppbv d$^{-1}$ is predicted at the surface and an O$_3$ loss rate of $\sim$3.59 ppbv d$^{-1}$ at the top of the MBL ($\sim$1 km). Although these analyses only consider the chemical processes that lead to a loss in O$_3$ and neglect physical processes, such as surface deposition and

entrainment of O$_3$, which can modify the overall O$_3$ destruction, this work demonstrates the increase in HO$_2$ and BrO concentrations is sufficient to compensate for the loss of IO at the higher altitudes. Aircraft measurements of HO$_2$ made over the Pacific during the Transport and Chemical Evolution over the Pacific (TRACE-P) campaign (Cantrell et al., 2003) provides some evidence that HO$_2$ concentrations increase over the first couple of kilometres. However, it is difficult to draw strong conclusions from the dataset due to the limited number of boundary layer observations that were made. Leser et al. (2003) have reported MAX-DOAS measurements of BrO taken onboard the R/V Polarstern north of the Canary Islands. Significant boundary layer BrO was observed, of the order of 1 pptv, although the vertical distribution within the boundary layer cannot be determined. Future, simultaneous observations of O$_3$, HO$_2$ and halogen oxides from 0–1 km from an aircraft platform, therefore, would be extremely beneficial.

Methane is removed from the atmosphere through oxidation by OH (Levy, 1971) with $\sim$25% of this removal occurring in the tropical MBL (Bloss et al., 2005a). In this work the important parameters which control the OH concentration in this region have been quantified, a number of which, until recently, have been overlooked, for example chemical processes involving halogen species. Although the vertical extent in the MBL of the impact of halogen oxides on the HO$_x$ and O$_3$ budgets, particularly for IO, remains uncertain, these species constitute a significant source of OH. Photolysis of HOBr and HOI lead to an increase in the OH concentration of $\sim$12%, although this increase is offset slightly ($\sim$3%) by the perturbation of the NO$_x$ chemistry (lowering [NO]) by halogen oxides as discussed in Sect. 3.4.2 Overall, this work suggests that the methane lifetime is reduced by $\sim$9%, due to the presence of halogen

oxides leading to an increase in [OH]. In the current atmosphere, one added methane molecule absorbs infra-red radiation ∼25 times more efficiently than one additional CO$_2$ molecule (Lelieveld et al., 1993) as CO$_2$ is approximately 200 times more abundant in the atmosphere and, as a consequence, many of its absorption bands are saturated. Current estimates suggest that methane contributes a radiative forcing of +0.48 (±0.05) Wm$^{-2}$ (Forster et al., 2007), which is ∼33% of that due to CO$_2$. Radiative forcing from methane increases approximately as the square root of its concentration (Forster et al., 2007), and it is estimated that without halogen oxides, the lower [OH] would lead to an increase in the radiative forcing by methane by ∼3.5×10$^{-3}$ Wm$^{-2}$. A key remaining question is the range of altitudes over which halogen oxides, particularly IO, extend. To fully determine the global impact of the halogen oxides on the oxidising capacity of the tropical BL, manifested through their effect on [OH], the vertical profile of these species in this region is required.

## 5 Summary

Measurements of OH and HO$_2$ radicals, together with a suite of supporting measurements, were made at the Cape Verde Atmospheric Observatory on the island of Sao Vicente during May and June 2007.

A model using the Master Chemical Mechanism, and constrained to the supporting measurements, was used to predict OH and HO$_2$ concentrations and to probe the chemistry controlling the radicals at the observatory. The halogen oxides, despite their low concentrations, were found to act as a significant HO$_2$ sink (19%), with the subsequent photolysis of the hypohalous acids increasing the modelled [OH]. The model was able to capture daytime radical concentration reasonably well, with the model falling within the 1 $\sigma$ measurement uncertainty of 20%. During the night, the model significantly under-predicts [HO$_2$], we suggest that the thermolysis of 100 pptv of PAN, entrained from the cooler air aloft could account for the model-measurement discrepancy at this time.

Active halogen chemistry over the tropical oceans, where photochemical oxidation is most prevalent, can significantly impact the global oxidising capacity via its effect on [OH]. From this work, the calculated methane lifetime could be as much as 9% shorter in this region if halogen chemistry is included in the calculation of [OH]. Currently, halogen chemistry is not routinely included in chemistry-transport models used to predict, for example, global distributions of tropospheric methane and O$_3$.

Further measurements of OH and HO$_2$ coupled with concurrent measurements of halogen oxides, VOCs, HCHO, HONO, NO$_x$, NO$_y$ and aerosol number and size distributions are needed to describe the chemistry of this region more fully and further test the hypotheses raised here. Vertical

profiles of the concentrations of IO, BrO, OH, HO$_2$ and O$_3$ are needed to discover if halogen chemistry has an impact on the budgets of OH, HO$_2$ and O$_3$ throughout the boundary layer.

## References

Abbatt, J. P. D. and Waschewsky, G. C. G.: Heterogeneous interactions of HOBr, HNO$_3$, O$_3$, and NO$_2$ with deliquescent NaCl aerosols at room temperature, J. Phys. Chem. A, 102, 3719–3725, 1998.

Alicke, B., Hebestreit, K., Stutz, J., and Platt, U.: Iodine oxide in the marine boundary layer, Nature, 397, 572–573, 1999.

Allan, B. J., McFiggans, G., Plane, J. M. C., and Coe, H.: Observations of iodine monoxide in the remote marine boundary layer, J. Geophys. Res.- Atmos., 105, 14363–14369, 2000.

Allan, J. D., Topping, D. O., Good, N., Irwin, M., Flynn, M., Williams, P. I., Coe, H., Baker, A. R., Martino, M., Niedermeier, N., Wiedensohler, A., Lehmann, S., Müller, K., Herrmann, H., and McFiggans, G.: Composition and properties of atmospheric particles in the eastern Atlantic and impacts on gas phase uptake rates, Atmos. Chem. Phys., 9, 9299–9314, 2009,
http://www.atmos-chem-phys.net/9/9299/2009/.

Ayers, G. P., Penkett, S. A., Gillett, R. W., Bandy, B., Galbally, I. E., Meyer, C. P., Elsworth, C. M., Bentley, S. T., and Forgan, B. W.: The annual cycle of peroxides and ozone in marine air at Cape Grim, Tasmania, J. Atmos. Chem., 23, 221-252, 1996.

Bielski, B. H. J.: Re-Evaluation of Spectral and Kinetic-Properties of HO$_2$ and O$_2^-$ Free-Radicals, Photochem. Photobiol., 28, 645–649, 1978.

Bloss, W. J., Evans, M. J., Lee, J. D., Sommariva, R., Heard, D. E., and Pilling, M. J.: The oxidative capacity of the troposphere: Coupling of field measurements of OH and a global chemistry transport model, Faraday Discuss., 130, 425–436, 2005a.

Bloss, W. J., Lee, J. D., Johnson, G. P., Sommariva, R., Heard, D. E., Saiz-Lopez, A., Plane, J. M. C., McFiggans, G., Coe, H., Flynn, M., Williams, P., Rickard, A. R., and Fleming, Z. L.: Impact of halogen monoxide chemistry upon boundary layer OH and HO$_2$ concentrations at a coastal site, Geophys. Res. Lett., 32, L06814, doi:10.1029/2004GL022084, 2005b.

Bloss, W. J., Lee, J. D., Heard, D. E., Salmon, R. A., Bauguitte, S. J.-B., Roscoe, H. K., and Jones, A. E.: Observations of OH and HO$_2$ radicals in coastal Antarctica, Atmos. Chem. Phys., 7, 4171–4185, 2007,
http://www.atmos-chem-phys.net/7/4171/2007/.

Brasseur, G. P., Hauglustaine, D. A., Walters, S., Rasch, P. J., Muller, J. F., Granier, C., and Tie, X. X.: MOZART, a global chemical transport model for ozone and related chemical tracers, 1. Model description, J. Geophys. Res.-Atmos., 103, 28265–28289, 1998.

Brauers, T., Hausmann, M., Bister, A., Kraus, A., and Dorn, H. P.: OH radicals in the boundary layer of the Atlantic Ocean, 1. Measurements by long-path laser absorption spectroscopy, J. Geophys. Res.-Atmos., 106, 7399–7414, 2001.

Bridier, I., Caralp, F., Loirat, H., Lesclaux, R., Veyret, B., Becker, K. H., Reimer, A., and Zabel, F.: Kinetic and theoretical studies of the reactions CH$_3$C(O)O$_2$+NO$_2$+M$\longleftrightarrow$CH$_3$C(O)O$_2$NO$_2$+M between 248 and 393 K and between 30–760 torr, J. Phys. Chem., 95, 3594–3600, 1991.

Cantrell, C. A., Edwards, G. D., Stephens, S., Mauldin, R. L., Zondlo, M. A., Kosciuch, E., Eisele, F. L., Shetter, R. E., Lefer, B. L., Hall, S., Flocke, F., Weinheimer, A., Fried, A., Apel, E., Kondo, Y., Blake, D. R., Blake, N. J., Simpson, I. J., Bandy, A. R., Thornton, D. C., Heikes, B. G., Singh, H. B., Brune, W. H., Harder, H., Martinez, M., Jacob, D. J., Avery, M. A., Barrick, J. D., Sachse, G. W., Olson, J. R., Crawford, J. H., and Clarke, A. D.: Peroxy radical behavior during the Transport and Chemical Evolution over the Pacific (TRACE-P) campaign as measured aboard the NASA P-3B aircraft, J. Geophys. Res.-Atmos., 108(D20), 8797, doi:10.1029/2003JD003674, 2003.

Carpenter, L. J., Monks, P. S., Bandy, B. J., Penkett, S. A., Galbally, I. E., and Meyer, C. P.: A study of peroxy radicals and ozone photochemistry at coastal sites in the northern and southern hemispheres, J. Geophys. Res.-Atmos., 102, 25417–25427, 1997.

Carpenter, L. J., Sturges, W. T., Penkett, S. A., Liss, P. S., Alicke, B., Hebestreit, K., and Platt, U.: Short-lived alkyl iodides and bromides at Mace Head, Ireland: Links to biogenic sources and halogen oxide production, J. Geophys. Res.-Atmos., 104, 1679–1689, 1999.

Carpenter, L. J., Lewis, A. C., Hopkins, J. R., Read, K. A., Longley, I. D., and Gallagher, M. W.: Uptake of methanol to the North Atlantic Ocean surface, Global Biogeochem. Cy., 18, 4, doi:10.1029/2004GB002294, 2004.

Chameides, W. L. and Davis, D.: Iodine – its possible role in tropospheric photochemistry, J. Geophys. Res.-Atmos., 85, 7383–7398, 1980.

Chang, W., Heikes, B., and Lee, M.: Ozone deposition to the sea surface: chemical enhancement and wind speed dependence, Atmos. Environ., 38, 1053–1059, 2004.

Chen, G., Davis, D., Crawford, J., Heikes, B., O'Sullivan, D., Lee, M., Eisele, F., Mauldin, L., Tanner, D., Collins, J., Barrick, J., Anderson, B., Blake, D., Bradshaw, J., Sandholm, S., Carroll, M., Albercook, G., and Clarke, A.: An assessment of HO$_X$ chemistry in the Tropical Pacific Boundary Layer: Comparison of model simulations with observations recorded during PEM Tropics A, J. Atmos. Chem., 38, 317–344, 2001.

Commane, R.: Understanding radical chemistry throughout the troposphere using laser-induced fluorescence spectroscopy, University of Leeds, 2009.

Curtis, A. R. and Sweetenham, W. P.: FACSIMILE/CHEKMAT users manual, in: Her majesty's stn. off., edited by: AERER12805, Norwich, England, 1987.

Dickerson, R. R., Rhoads, K. P., Carsey, T. P., Oltmans, S. J., Burrows, P. J., and Crutzen, P. J.: Ozone in the remote marine boundary layer: A possible role for halogens, J. Geophys. Res.-Atmos., 104, 21385–21395, 1999.

Fairall, C. W., Hare, J. E., Edson, J. B., and McGillis, W.: Parameterization and micrometeorological measurement of air-sea gas transfer, Bound.-Lay. Meteorol., 96, 63–105, 2000.

Fairall, C. W., Helmig, D., Ganzeveld, L., and Hare, J.: Waterside turbulence enhancement of ozone deposition to the ocean, Atmos. Chem. Phys., 7, 443–451, 2007, http://www.atmos-chem-phys.net/7/443/2007/.

Fleming, Z. L., Monks, P. S., Rickard, A. R., Heard, D. E., Bloss, W. J., Seakins, P. W., Still, T. J., Sommariva, R., Pilling, M. J., Morgan, R., Green, T. J., Brough, N., Mills, G. P., Penkett, S. A., Lewis, A. C., Lee, J. D., Saiz-Lopez, A., and Plane, J. M. C.: Peroxy radical chemistry and the control of ozone photochemistry at Mace Head, Ireland during the summer of 2002, Atmos. Chem. Phys., 6, 2193–2214, 2006, http://www.atmos-chem-phys.net/6/2193/2006/.

Furneaux, K. L., Whalley, L. K., Heard, D. E., Atkinson, H. M., Bloss, W. J., Flynn, M. J., Gallagher, M. W., Ingham, T., Kramer, L., Lee, J. D., Leigh, R., McFiggans, G. B., Mahajan, A. S., Monks, P. S., Oetjen, H., Plane, J. M. C., and Whitehead, J. D.: Measurements of iodine monoxide at a semi polluted coastal location, Atmos. Chem. Phys. Discuss., 9, 25737–25797, 2009, http://www.atmos-chem-phys-discuss.net/9/25737/2009/.

Galbally, I. E., Bentley, S. T., and Meyer, C. P.: Mid-latitude marine boundary layer ozone destruction at visible sunrise observed at Cape Grim, Tasmania, 41 degrees S, Geophys. Res. Lett., 27, 3841, doi:10.1029/1999GL010943, 2000.

Gallagher, M. S., Carsey, T. P., and Farmer, M. L.: Peroxyacetyl nitrate in the north Atlantic marine boundary layer, Global Biogeochem. Cy., 4, 297–308, 1990.

Ganzeveld, L. and Lelieveld, J.: Dry Deposition Parameterization in a Chemistry General-Circulation Model and Its Influence on the Distribution of Reactive Trace Gases, J. Geophys. Res.-Atmos., 100, 20999–21012, 1995.

Haggerstone, A.-L., Carpenter, L. J., Carslaw, N., and McFiggans, G.: Improved model predictions of HO$_2$ with gas to particle mass transfer rates calculated using aerosol number size distribution, J. Geophys. Res.-Atmos., 110(D4), D04304, doi:10.1029/2004JD005282, 2005.

Heard, D. E. and Pilling, M. J.: Measurement of OH and HO$_2$ in the Tropopshere, Chem. Rev., 103, 5163–5198, 2003.

Hoell, J. M., Davis, D., Liu, S., Newell, R. E., Shipman, M., Akimoto, H., McNeal, R. J., Bendura, R. J., and Drewry, J. W.: Pacific Exploratory Mission-West A (PEM-West A) September–October 1991, J. Geophys. Res.-Atmos., 101, 1641–1653, 1996.

Hoell, J. M., Davis, D., Liu, S., Newell, R. E., Akimoto, H., McNeal, R. J., and Bendura, R. J.: The Pacific Exploratory Mission-West Phase B: February–March 1994, J. Geophys. Res.-Atmos., 102, 28223–28239, 1997.

Hoell, J. M., Davis, D., Jacob, D. J., Rodgers, M. O., Newell, R. E., Fuelberg, H. E., McNeal, R. J., Raper, J. L., and Bendura, R. J.: Pacific Exploratory Mission in the tropical Pacific: PEM-Tropics A, August–September 1996, J. Geophys. Res.-Atmos., 104, 5567–5583, 1999.

Hough, A. M.: The calculation of photolysis rates for use in global tropospheric modelling studies, AERE rep., Her Majesty's Stn. Off., Norwich, 1988.

IUPAC: http://www.iupac-kinetic.ch.cam.ac.uk/, last access: 8 July 2009, 2006.

Jacobi, H.-W., Weller, R., Bluszcz, T., and Schrems, O.: Latitudinal distribution of peroxyacetyl nitrate (PAN) over the Atlantic ocean, J. Geophys. Res.-Atmos., 104, 26901–26912, 1999.

Junkermann, W. and Stockwell, W. R.: On the budget of photooxidants in the marine boundary layer of the tropical South Atlantic, J. Geophys. Res.-Atmos., 104, 8039–8046, 1999.

Kanaya, Y., Cao, R., Kato, S., Miyakawa, Y., Kajii, Y., Tanimoto, H., Yokouchi, Y., Mochida, M., Kawamura, K., and Akimoto, H.: Chemistry of OH and HO$_2$ radicals observed at Rishiri Island, Japan, in September 2003: Missing daytime sink of HO$_2$ and positive nighttime correlations with monoterpenes, J. Geophys. Res.-Atmos., 112, D11308, doi:10.1029/2006JD007987, 2007.

Keene, W. C., Long, M. S., Pszenny, A. A. P., Sander, R., Maben, J. R., Wall, A. J., O'Halloran, T. L., Kerkweg, A., Fischer, E. V., and Schrems, O.: Latitudinal variation in the multiphase chemical processing of inorganic halogens and related species over the eastern North and South Atlantic Oceans, Atmos. Chem. Phys., 9, 7361–7385, 2009,
http://www.atmos-chem-phys.net/9/7361/2009/.

Lee, J. D., McFiggans, G., Allan, J. D., Baker, A. R., Ball, S. M., Benton, A. K., Carpenter, L. J., Commane, R., Finley, B. D., Evans, M., Fuentes, E., Furneaux, K., Goddard, A., Good, N., Hamilton, J. F., Heard, D. E., Herrmann, H., Hollingsworth, A., Hopkins, J. R., Ingham, T., Irwin, M., Jones, C. E., Jones, R. L., Keene, W. C., Lawler, M. J., Lehmann, S., Lewis, A. C., Long, M. S., Mahajan, A., Methven, J., Moller, S. J., Müller, K., Müller, T., Niedermeier, N., O'Doherty, S., Oetjen, H., Plane, J. M. C., Pszenny, A. A. P., Read, K. A., Saiz-Lopez, A., Saltzman, E. S., Sander, R., von Glasow, R., Whalley, L., Wiedensohler, A., and Young, D.: Reactive Halogens in the Marine Boundary Layer (RHaMBLe): the tropical North Atlantic experiments, Atmos. Chem. Phys., 10, 1031–1055, 2010,
http://www.atmos-chem-phys.net/10/1031/2010/.

Lee, J. D., Moller, S. J., Read, K. A., Lewis, A. C., Mendes, L., and Carpenter, L. J.: Year round measurements of nitrogen oxides and ozone in the tropical North Atlantic marine boundary layer, J. Geophys. Res., 114, D21, doi:10.1029/2009JD011878, 2009.

Lelieveld, J., Crutzen, P. J., and Bruhl, C.: Climate effects of atmospheric methane, Chemosphere, 26, 739–768, 1993.

Leser, H., Honninger, G., and Platt, U.: MAX-DOAS measurements of BrO and NO$_2$ in the marine boundary layer, Geophys. Res. Lett., 30, 1537, doi:10.1029/2002GL015811, 2003.

Levy, H.: Normal atmosphere: Large radical and formaldehyde concentrations predicted, Science, 173, 141–143, 1971.

Mahajan, A. S., Plane, J. M. C., Oetjen, H., Whalley, L., Furneaux, K., Ingham, T., Heard, D., and Saiz-Lopez, A.: Long term DOAS observations of formaldehyde over the tropical Atlantic Ocean in preparation, in preparation, 2010.

Mauldin III, R. L., Tanner, D., and Eisele, F.: Measurements of OH during PEM-Tropics A, J. Geophys. Res.-Atmos., 104, 5817–5827, 1999.

Mauldin III, R. L., Eisele, F., Cantrall, C., Kosciuch, E., Ridley, B. A., Lefer, B., Tanner, D., Nowak, J. B., Chen, G., Wang, L., and Davis, D.: Measurements of OH aboard the NASA P-3 during PEM-Tropics B, J. Geophys. Res.-Atmos., 106, 32657–32666, 2001.

MCM: Master Chemical Mechanism, Version 3.1, http://mcm.leeds.ac.uk/MCM/home, last access: 08 July 2009.

Monks, P. S., Carpenter, L. J., Penkett, S. A., Ayers, G. P., Gillett, R. W., Galbally, I. E., and Meyer, C. P.: Fundamental ozone photochemistry in the remote marine boundary layer: The SOAPEX experiment, measurement and theory, Atmos. Environ., 32, 3647–3664, 1998.

Moore, R., Oram, D., and Penkett, S. A.: Production of isoprene by marine phytoplankton cultures, Geophys. Res. Lett., 21, 2507–2510, 1994.

Mossinger, J. C. and Cox, R. A.: Heterogeneous reaction of HOI with sodium halide salts, J. Phys. Chem. A, 105, 5165–5177, 2001.

Müller, K. P. and Rudolph, J.: Measurements of peroxyacetylnitrate in the marine boundary layer over the Atlantic, J. Atmos. Chem., 15, 3–4, 1992.

Pechtl, S., Schmitz, G., and von Glasow, R.: Modelling iodide - iodate speciation in atmospheric aerosol: Contributions of inorganic and organic iodine chemistry, Atmos. Chem. Phys., 7, 1381–1393, 2007,
http://www.atmos-chem-phys.net/7/1381/2007/.

Penkett, S. A., Monks, P. S., Carpenter, L. J., Clemitshaw, K. C., Ayers, G. P., Gillett, R. W., Galbally, I. E., and Meyer, C. P.: Relationship between ozone photolysis rates and peroxy radical concentrations in clean marine air over the Southern Ocean, J. Geophys. Res.-Atmos., 102, 12805–12817, 1997.

Plane, J. M. C. and Saiz-Lopez, A.: UV-Visible Differential Optical Absorption Spectroscopy (DOAS), in: Analytical Techniques for Atmospheric Measurements, edited by: Heard, D. E., Blackwell Publishing, 147–180 pp., 2006.

Plane, J. M. C.: Personal Communication, 2009.

Poppe, D.: Time constant analysis of tropospheric gas-phase chemistry, Phys. Chem. Chem. Phys., 1, 5417–5422, 1999.

Raper, J. L., Kleb, M. M., Jacob, D. J., Davis, D., Newell, R. E., Fuelberg, H. E., Bendura, R. J., Hoell, J. M., and McNeal, R. J.: Pacific Exploratory Mission in the Tropical Pacific: PEM-Tropics B, March–April 1999, J. Geophys. Res.-Atmos., 106, 32401–32425, 2001.

Ravishankara, A. R.: Heterogeneous and multiphase chemistry in the troposphere, Science, 276, 1058–1065, 1997.

Read, K. A., Mahajan, A. S., Carpenter, L. J., Evans, M. J., Faria, B. V. E., Heard, D. E., Hopkins, J. R., Lee, J. D., Moller, S. J., Lewis, A. C., Mendes, L., McQuaid, J. B., Oetjen, H., Saiz-Lopez, A., Pilling, M. J., and Plane, J. M. C.: Extensive halogen-mediated ozone destruction over the tropical Atlantic Ocean, Nature, 453, 1232–1235, 2008.

Read, K. A., Lee, J. D., Lewis, A. C., Moller, S. J., Neves, L. M., and Carpenter, L. J.: Intra-annual cycles of NMVOC in the tropical marine boundary layer and their use for interpreting seasonal variability in CO, J. Geophys. Res., 114, D21, doi:10.1029/2009JD011879, 2009.

Read, K. A., Lewis, A. C., Mendes, L., Whalley, L. K., and Carpenter, L. J.: VOCs in the tropical remote marine boundary layer: Trends, ocean influence and atmospheric impacts, in preparation, 2010.

Saiz-Lopez, A. and Plane, J. M. C.: Novel iodine chemistry in the marine boundary layer, Geophys. Res. Lett., 31, 4, doi:10.1029/2003GL09215, 2004a.

Saiz-Lopez, A., Plane, J. M. C., and Shillito, J.: Bromine oxide in the mid-latitude marine boundary layer, Geophys. Res. Lett., 31(3), L03111, doi:10.1029/2003GL018956, 2004b.

Salisbury, G., Rickard, A. R., Monks, P. S., Allan, B. J., Bauguitte, S., Penkett, S. A., Carslaw, N., Lewis, A. C., Creasey, D. J., Heard, D. E., Jacobs, P. J., and Lee, J. D.: Production of peroxy radicals at night via reactions of ozone and the nitrate radical in the marine boundary layer, J. Geophys. Res.-Atmos., 106, 12669–12687, 2001.

Sander, R.: Modeling atmospheric chemistry: interactions between gas-phase species and liquid cloud/aerosols particles, Surv. Geophys., 20, 1–31, 1999.

Saunders, S. M., Jenkin, M. E., Derwent, R. G., and Pilling, M. J.: Protocol for the development of the Master Chemical Mechanism, MCM v3 (Part A): tropospheric degradation of non-aromatic volatile organic compounds, Atmos. Chem. Phys., 3, 161–180, 2003,
http://www.atmos-chem-phys.net/3/161/2003/.

Schwartz, S. E.: Gas-Phase and Aqueous-Phase Chemistry of HO$_2$ in Liquid Water Clouds, J. Geophys. Res.-Atmos., 89, 1589–1598, 1984.

Shaw, S. L., Chisholm, S. W., and Prinn, R. G.: Isoprene production by Prochlorococcus, a marine cyanobacterium and other phytoplankton, Mar. Chem., 80, 227–245, 2003.

Singh, H. B., Chen, Y., Staudt, A., Jacob, D., Blake, D., Heikes, B., and Snow, J.: Evidence from the Pacific troposphere for large global sources of oxygenated organic commpounds, Nature, 410, 1078–1081, 2001.

Singh, H. B., Tabazadeh, A., Evans, M. J., Field, B. D., Jacob, D. J., Sachse, G., Crawford, J. H., Shetter, R., and Brune, W. H.: Oxygenated volatile organic chemicals in the oceans: Inferences and implications based on atmospheric observations and air-sea exchange models, Geophys. Res. Lett., 30(16), 1862, doi:10.1029/2003GL017933, 2003.

Smith, S. C., Lee, J. D., Bloss, W. J., Johnson, G. P., Ingham, T., and Heard, D. E.: Concentrations of OH and HO$_2$ radicals during NAMBLEX: measurements and steady state analysis, Atmos. Chem. Phys., 6, 1435–1453, 2006,
http://www.atmos-chem-phys.net/6/1435/2006/.

Smith, S. C. Atmospheric measurements of OH and HO$_2$ using the FAGE technique: Instrument development and data analysis, University of Leeds, 2007.

Sommariva, R., Haggerstone, A.-L., Carpenter, L. J., Carslaw, N., Creasey, D. J., Heard, D. E., Lee, J. D., Lewis, A. C., Pilling, M. J., and Zádor, J.: OH and HO$_2$ chemistry in clean marine air during SOAPEX-2, Atmos. Chem. Phys., 4, 839–856, 2004,
http://www.atmos-chem-phys.net/4/839/2004/.

Sommariva, R., Bloss, W. J., Brough, N., Carslaw, N., Flynn, M., Haggerstone, A.-L., Heard, D. E., Hopkins, J. R., Lee, J. D., Lewis, A. C., McFiggans, G., Monks, P. S., Penkett, S. A., Pilling, M. J., Plane, J. M. C., Read, K. A., Saiz-Lopez, A., Rickard, A. R., and Williams, P. I.: OH and HO$_2$ chemistry during NAMBLEX: roles of oxygenates, halogen oxides and heterogeneous uptake, Atmos. Chem. Phys., 6, 1135–1153, 2006,
http://www.atmos-chem-phys.net/6/1135/2006/.

Stull, R. B.: Introduction to Boundary Layer Meteorology, Publishers, K. A., Dordrecht, 1988.

Taketani, F., Kanaya, Y., and Akimoto, H.: Kinetcis of heterogeneous reactions of HO$_2$ radical at ambient concentration levels with (NH$_4$)$_2$SO$_4$ and NaCl aerosol particles, J. Phys. Chem. A, 112, 2370–2377, 2008.

Taketani, F., Kanaya, Y., and Akimoto, H.: Heterogeneous loss of HO$_2$ by KCl, synthetic sea salt, and natural seawater aerosol particles, Atmos. Environ., 43, 1660–1665, 2009.

Thornton, J. A., Jaegle, L., and McNeill, V. F.: Assessing known pathways for HO$_2$ loss in aqueous atmospheric aerosols: Regional and global impacts on tropospheric oxidants, J. Geophys. Res.-Atmos., 113, D05303, doi:10.1029/2007JD009236, 2008.

Vogt, R., Crutzen, P. J., and Sander, R.: A mechanism for halogen release from sea-salt aerosol in the remote marine boundary layer, Nature, 383, 327–330, 1996.

Vogt, R., Sander, R., von Glasow, R., and Crutzen, P. J.: Iodine chemistry and its role in halogen activation and ozone loss in the marine boundary layer: A model study, J. Atmos. Chem., 32, 375, doi:10.1023/A:1006179901037, 1999.

von Glasow, R. and Sander, R.: Variation of sea salt aerosol pH with relative humidity, Geophys. Res. Lett., 28, 247–250, 2001.

von Glasow, R., Sander, R., Bott, A., and Crutzen, P. J.: Modelling halogen chemistry in the marine boundary layer – 1. Cloud-free MBL, J. Geophys. Res.-Atmos., 107, 4341, doi:10.1029/2001JD000942, 2002.

von Glasow, R., von Kuhlmann, R., Lawrence, M. G., Platt, U., and Crutzen, P. J.: Impact of reactive bromine chemistry in the troposphere, Atmos. Chem. Phys., 4, 2481–2497, 2004,
http://www.atmos-chem-phys.net/4/2481/2004/.

von Glasow, R.: Personal Communication, 2009.

Wachsmuth, M., Gäggeler, H. W., von Glasow, R., and Ammann, M.: Accommodation coefficient of HOBr on deliquescent sodium bromide aerosol particles, Atmos. Chem. Phys., 2, 121–131, 2002,
http://www.atmos-chem-phys.net/2/121/2002/.

Weller, R., Schrems, O., Boddenberg, A., Gäb, S., and Gautrois, M.: Meridional distribution of hydroperoxides and formaldehyde in the marine boundary layer of the Atlantic (48° N–35° S) measured during the Albatross campaign, J. Geophys. Res.-Atmos. ,105, 14401–14412, 2000.

Whalley, L. K., Furneaux, K. L., Gravestock, T., Atkinson, H. M., Bale, C. S. E., Ingham, T., Bloss, W. J., and Heard, D. E.: Detection of iodine monoxide radicals in the marine boundary layer using laser induced fluorescence spectroscopy, J. Atmos. Chem., 58, 19–39, 2007.